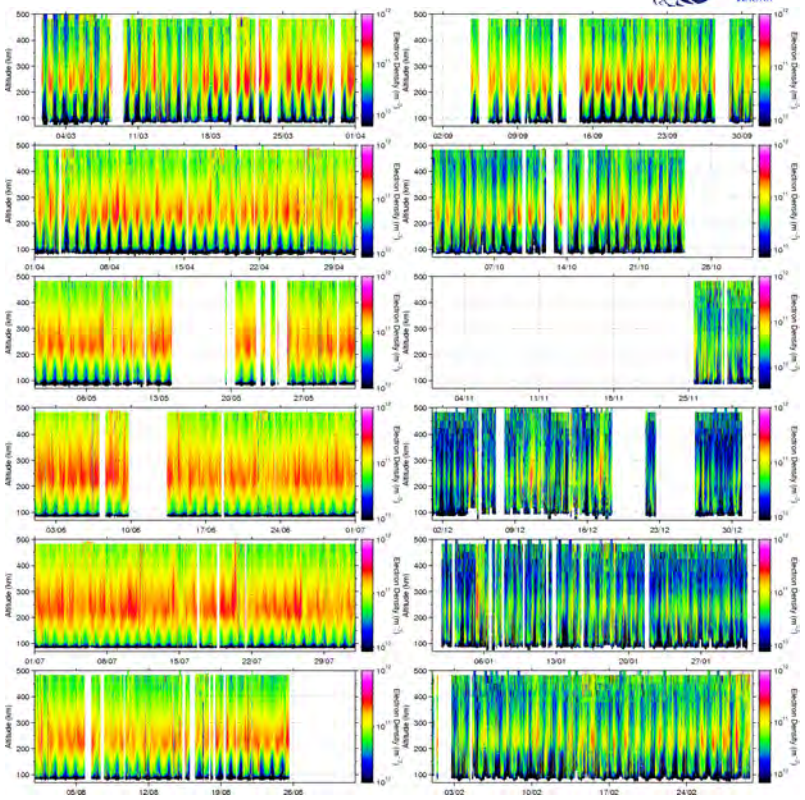

EISCAT

EUROPEAN INCOHERENT SCATTER SCIENTIFIC ASSOCIATION

ANNUAL REPORT 2008

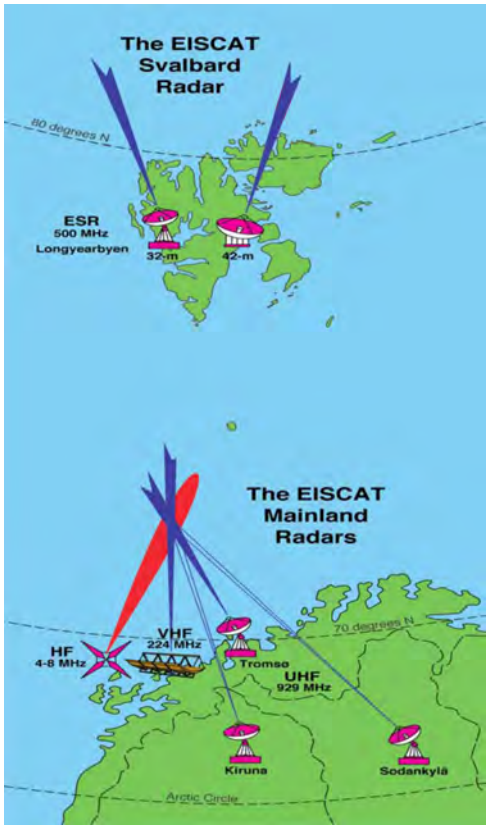

EISCAT Radar Systems

Location	Tromsø		Kiruna	Sodankylä	Longyearbyen	
Geographic coordinates	69°35′N 19°14′E		67°52′N 20°26′E	67°22′N 26°38′E	78°09′N 16°02′E	
Geomagnetic inclination	77°30′N		76°48′N	76°43′N	82°06′N	
Invariant latitude	66°12′N		64°27′N	63°34′N	75°18′N	
Band	VHF	UHF	UHF	UHF	UHF	
Frequency (MHz)	224	931	931	931	500	
Maximum bandwidth (MHz)	3	8	8	8	10	
Transmitter	2 klystrons	2 klystrons	-	-	16 klystrons	
Channels	8	8	8	8	6	
Peak Power (MW)	2×1.5	2×1.3	-	-	1.0	
Average power (MW)	2×0.19	2×0.16	-	-	0.25	
Pulse duration (ms)	0.001–2.0	0.001–2.0	-	-	<0.001–2.0	
Phase coding	binary	binary	binary	binary	binary	
Minimum interpulse (ms)	1.0	1.0	-	-	0.1	
Receiver	analog	analog	analog	analog	analog-digital	
System temperature (K)	250–300	90–110	30–35	30–35	55–65	
Digital processing	14 bit ADC, 32 bit complex, autocorrelation functions, parallel channels				12 bit ADC, lag profiles 32 bit complex	
					Antenna 1	**Antenna 2**
Antenna	parabolic cylinder 120 m×40 m steerable	parabolic dish 32 m steerable	parabolic dish 32 m steerable	parabolic dish 32 m steerable	parabolic dish 32 m steerable	parabolic dish 42 m fixed
Feed system	line feed 128 crossed dipoles	Cassegrain	Cassegrain	Cassegrain	Cassegrain	Cassegrain
Gain (dBi)	46	48	48	48	42.5	45
Polarization	circular	circular	any	any	circular	circular

EISCAT Heating Facility in Tromsø

Frequency range: 4–8 MHz, Maximum transmitter power: 12×0.1 MW, Antennas: two arrays (4–8 MHz): 24 dBi, one array (5.4–8 MHz): 30 dBi. Additionally, a Dynasonde is operated at the Heating facility.

Cover picture: One full year of electron density data from the ESR 42 m antenna.

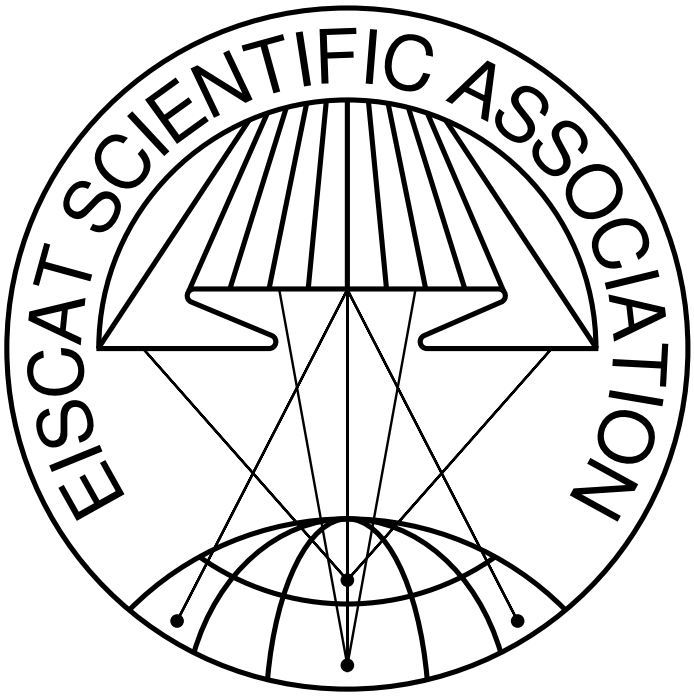

EISCAT Scientific Association
2008

EISCAT, the European Incoherent Scatter Scientific Association, is established to conduct research on the lower, middle and upper atmosphere and ionosphere using the incoherent scatter radar technique. This technique is the most powerful ground-based tool for these research applications. EISCAT is also being used as a coherent scatter radar for studying instabilities in the ionosphere, as well as for investigating the structure and dynamics of the middle atmosphere and as a diagnostic instrument in ionospheric modification experiments with the Heating facility.

There are ten incoherent scatter radars in the world, and EISCAT operates three of the highest-standard facilities. The experimental sites of EISCAT are located in the Scandinavian sector, north of the Arctic Circle. They consist of two independent radar systems on the mainland, together with a further radar constructed on the island of Spitzbergen in the Svalbard archipelago — the EISCAT Svalbard Radar — Scandinavia (see schematic and operating parameters on the inside of the front cover).

The EISCAT UHF radar operates in the 931 MHz band with a peak transmitter power of more than 2.0 MW and 32 m, fully steerable parabolic dish antennas. The transmitter and one receiver are in Tromsø (Norway). Receiving sites are also located near Kiruna (Sweden) and Sodankylä (Finland), allowing continuous tri-static measurements to be made.

The monostatic VHF radar in Tromsø operates in the 224 MHz band with a peak transmitter power of 2×1.5 MW and a 120 m $\times$ 40 m parabolic cylinder antenna, which is subdivided into four sectors. It can be steered mechanically in the meridional plane from vertical to 60° north of the zenith; limited east-west steering is also possible using alternative phasing cables.

The EISCAT Svalbard radar (ESR), located near Longyearbyen, operates in the 500 MHz band with a peak transmitter power of 1.0 MW, a fully steerable parabolic dish antenna of 32 m diameter, and a fixed field aligned antenna of 42 m diameter. The high latitude location of this facility is particularly aimed at studies of the cusp and polar cap region.

The basic data measured with the incoherent scatter radar technique are profiles of electron density, electron and ion temperature, and ion velocity. Subsequent processing allows a wealth of further parameters, describing the ionosphere and neutral atmosphere, to be derived. A selection of well-designed radar pulse schemes are available to adapt the data-taking routines to many particular phenomena, occurring at altitudes between about 50 km and more than 2000 km. Depending on geophysical conditions, a best time resolution of less than one second and an altitude resolution of a few hundred meters can be achieved.

Operations of 3–4000 hours each year are distributed equally between Common Programmes (CP) and Special Programmes (SP). At present, six well-defined Common Programmes are run regularly, for between one and three days, typically about once per month, to provide a data base for long term synoptic studies. A large number of Special Programmes, defined individually by Associate scientists, are run to support national and international studies of both specific and global geophysical phenomena.

Further details of the EISCAT system and operation can be found in various EISCAT reports, including illustrated brochures, which can be obtained from EISCAT Headquarters in Kiruna, Sweden.

The investments and operational costs of EISCAT are shared between:

China Research Institute of Radiowave Propagation, Peoples Republic of China
Deutsche Forschungsgemeinschaft, Germany
National Institute of Polar Research, Japan
Norges forskningsråd, Norway
Science and Technology Facilities Council, UK
Solar-Terrestrial Environment Laboratory, Nagoya University, Japan
Suomen Akatemia, Finland
Vetenskapsrådet, Sweden

Contents

The chairman's section

February 29, 2008 marked the end of the longest run ever conducted by the EISCAT incoherent scatter radar system. This was the one year run by the ESR devoted to IPY. The impressive database derived during this yearlong experiment is expected to contribute in a significant manner to a better understanding and improved modeling of the polar upper atmosphere. We are extremely grateful to the EISCAT staff for devoting themselves to this effort and making it such a great success.

2008 also marked the first year when EISCAT was without a deputy director as Dr. Gudmund Wanberg left EISCAT on February 29 to join the staff at IRF. Dr. Wannberg has served EISCAT for many years and especially his involvement in the establishment of the ESR has had a decisive impact on the successful operation of this facility. Dr. Wannberg also contributed strongly to the planning of the new EISCAT_3D system that obtained support for a feasibility funded by the EU 6th framework program. EISCAT staff and personell from the associates has endeavored themselves throughout 2008 to comply with the EU standards for such developments. Council at its fall meeting in Kunming endorsed The EISCAT_3D concept by resolving that the development of new radar facilities capable of three-dimensional volumetric imaging of the atmosphere and ionosphere is an essential requirement for the future of the association. During this meeting Council was also introduced to the Chinese plans of installing a third antenna at the ESR.

For the first time a staff representative was present at a Council meeting. It is hoped that this contact between the EISCAT staff and representatives from the associates will strengthen the spirit of community in the EISCAT organization.

The scientific outcome of the EISCAT activity in 2008 has been less than average and represents a trend in EISCAT science activity for the last 5 years or so. It is not easy to find a simple explanation for this reduced activity during the last years, but the fact that France has resigned from the organization and that Germany has much reduced its activity are elements that contribute to this development. However, French scientists still enjoy the opportunity to conduct EISCAT experiments using their national funding grants with annual experiment time-buying arrangements. A very positive new development is that we can welcome Ukraine from 2009 as an affiliate member and that Russia also has signed an agreement to use EISCAT facilities during the next 3 years.

From the reports presented by EISCAT scientists we notice that there is an increased activity in combining EISCAT radar measurements with observations based on other more traditional instruments such as optical, riometers and magnetometers etc. These combined activities strengthen the cooperation between research groups with different experimental background and is a positive development for the science community as a total. Plans for installing FPI instruments and LIDARS at EISCAT also contributes to this positive development. Studies of PMSE play an important part of the science work at EISCAT as well as meteor studies. The new activities in observations of space debris may bring the EISCAT scientists in contact with communities that normally do not consider EISCAT as an installation suited for their research. It is also good to see that the Heating facility is more actively used than for some time: especially the strong interest in PMSE studies contributes to this. The lunar radar mapping and the development of radar interferometry are activities demonstrating that EISCAT scientists are very innovative. The latter project is expected to play an important role in the development of EISCAT_3D.

2008 was a very difficult year both economically and administratively for EISCAT. The staff had to be reduced and the maintenance of the mainland installations had to suffer. When STFC in UK indicated that they would reduce their support to ground based research such as EISCAT and that they would transfer their responsibility to NERC, it was a great concern to the association.

At the end of 2007 it became clear that the engagement of Dr. Anthony van Eyken as a director would not be prolonged. EISCAT is very grate-

ful for the long time Dr. van Eyken has served the organisation and contributed to the development of the association in a most favorable way. Dr. van Eyken's indefatigable efforts to work for the future of EISCAT by proposing the EISCAT_3D project will stand out as a major achievement in the history of the association. The status of these future plans received a high-level political support in December 2008, when the proposal by the Swedish Research Council to include EISCAT_3D in the ESFRI Roadmap of large European research infrastructures was accepted by the European Strategy Forum on Research Infrastructures.

A search committee was set up an in the fall of the year. Dr. Esa Turunen was appointed to become director from 2009. On behalf of the EISCAT Council I am looking forward to a successful cooperation with Director Turunen and wish him all the best in his important position for the association.

As 2008 marked the end of my four year period as chairman of Council I would like to thank the EISCAT staff at EISCAT for their ability and benevolence to assist the scientists in their efforts to pursue ideas and wishes. I will also thank my colleagues in EISCAT Council for helping me to solve some of the challenging problems we had to face in 2008.

Prof. Asgeir Brekke
Chairman of the EISCAT Council

Director's pages

As 2008 closes, the EISCAT Scientific Association is in quite remarkable shape. Comparing the situation today with that of five or six years ago, when the Association and its user community were disheartened, were facing the very real prospect of closure and decommissioning, and had little or no planning for any future in place at all, with today, when the user community is showing real signs of resurgence, the future is full of opportunity and promise, and we have evolving plans for five, ten, and thirty years well under way, it is easy to see that this is true.

The 50th anniversary of the reception of the first incoherent scatter returns from the ionosphere by Ken Bowles, at Long Branch in Illinois, took place on 21 October. An amazing amount has happened in the field since then, many wonderful facilities have been constructed and operated in many countries, and many brilliant minds have contributed to the development of the theory, techniques, and hardware. Nevertheless, we are today arguably enjoying the most exciting period since those first echoes were received fifty years ago with the tremendous momentum now behind the EISCAT_3D initiative, the AMISR development lines in the US, and plans for new radars in China, in the Antarctic, and elsewhere.

2008 has been a busy year: in addition to the formal EISCAT member countries, France continues to use EISCAT facilities through an experiment time purchase arrangement. An agreement with the Russian Arctic and Antarctic Research Institute allows them to buy EISCAT time over the next four years, the first payment, of more than 200 k€, will be transferred to EISCAT before the end of the year and will be followed by similar payments in subsequent years. These funds will be primarily used to support two Heating/UHF campaigns a year. Formally we also expect Ukraine to join in the near future, but currently we have included only minimal nominal values in the budget forecast. The Third Party Access and EU-funded Trans-National Access programs have also continued throughout the year bringing a number of new users, from non-EISCAT countries, to the EISCAT facilities.

The UHF and VHF radars have operated as normal with occasional problems commensurate with systems of this age. The UHF GAsFET amplifier at Tromsø has been replaced by an un-cooled HEMT amplifier (as used at Kiruna and Sodankylä), without significantly increasing the system temperature, while one elevation drive motor failed and was replaced. The UHF frequency is still expected to be reallocated in the Sodankylä area at the end of 2009 though Tromsø and Kiruna may remain free beyond that date. Smart signal processing may allow operations at Sodankylä to continue even in the face of GSM interference.

The VHF radar is running satisfactorily with the single klystron. There has been some interference from DAB between 228.304 and 229.840 MHz but it should be possible to avoid that band. Given the good experience at UHF, the Tromsø staff want to try replacing the VHF front end with a HEMT unit too.

Heating has run a substantial amount during the year and the Heating upgrade work is also proceeding steadily. Most of the hardware for the heater upgrade is now in Tromsø, ready for further testing and software development. The digital part of the receiver is also on site, but some analogue parts still need to be obtained and assembled. The ex-BAS dynasonde has been received,

tested at Tromsø, shipped, and installed on Svalbard.

In Kiruna one of the azimuth drives developed a disturbing noise profile and movements were restricted until the problem could be fully investigated and corrected. With the help of a local railway engineer, the problem was localised to the outer bearing assembly on one of the driven wheels. The components were sourced and replacement completed (required jacking the antenna, though only about 70 tons needed to be supported) without any need to realign the drive chain. Subsequently the elevation shaft encoder failed but Tromsø had three spares on hand and one was quickly routed to Kiruna and installed. The antenna is operating effectively after a full calibration following the azimuth wheel bearing problem.

A computer cluster transferred to EISCAT from RAL has been installed at the Kiruna site. The purpose is to make user access (whether on site or remote) to the archived data much more elegant and support the application of these computer resources as a compute facility to work with the main data archive. For the first time, users will be able to make investigations and analyses using the entire archive and finally be able to exploit what we have for years acknowledged to be a data resource of immense value, potential, and utility. Once running on these systems, a new release of GUISDAP is planned; the main new feature from the users' viewpoint will be the routine derivation of three-dimensional velocity components. On the analysed data side, Bill Rideout, the main Madrigal support programmer at Millstone Hill, completed a visit to Kiruna during the year and updated Madrigal to the latest version.

The European Space Agency, ESA, has expressed a wish to restart the Space Debris project at Sodankylä but this can not be accomplished in the present year. However, if realized, the project should provide an opportunity to take on a further project engineer position supported by the new contract at Sodankylä.

At the EISCAT Svalbard Radar, ESR, the 32 m azimuth control developed problems related to drive motor six. The Siemens Company rapidly provided a replacement control card but it was not until some field modifications to that card, completed under the advice of Siemens engineers, had been made that the problem was finally cured and the antenna became fully operational again. The power station in Longyearbyen experienced further difficulties in the Autumn and was unable to provide power for radar operations during late August and most of September while the seawater pump system was replaced. On several occasions the entire valley load was taken by the new 1 MW generator at Mine 7, but of course this provided no power for active transmitter operations or to move the antenna.

The EISCAT_3D Design Study absorbed much staff effort during the year. Shortly after the end-of-third period report was submitted to Brussels, all the paperwork required to introduce IRF, Kiruna, as a fifth partner, and to make some other smaller changes to resource allocations, were also submitted to Brussels and subsequently accepted and implemented. There is no reason why the EISCAT_3D Design Project should not complete on time and produce a very acceptable final product.

A formal proposal covering the EISCAT_3D system was submitted to the ESFRI roadmap revision exercise by the Swedish ESFRI delegation almost exactly one year ago. The ESR was also included in a Norwegian submission "Svalbard Integrated Arctic Earth Observing System" — SIAEOS. Professor Carlo Rizzuto (Chairman, ESFRI) and Hervé Pero (Secretary ESFRI, Head of Unit Research Infrastructures, EC), the two heads of ESFRI, visited Svalbard around 22 August and Gunnar Sand, the UNIS Director, and I gave them formal presentations on UNIS/SIAEOS and EISCAT/EISCAT_3D respectively.

The outcome was that EISCAT_3D was indeed included in the revised ESFRI roadmap as formally announced at the European Conference on Research Infrastructures (ECRI) in Versailles on the 9th and 10th December. The SIAEOS proposal is also included in the ESFRI roadmap, so a lot has certainly been achieved in raising awareness of EISCAT in the European Community — all in advance of the publication of the technical parts of the Design Study which should provide tremendous further impetus of course. The EISCAT_3D design exercise is already a success and the probability that EISCAT *can*, maybe in truth it would be better to say *must*, now build the system is really high. The EISCAT Council, technical project leader Gudmund Wannberg, our partners, and the EISCAT staff can be really proud that this has come to pass on our watch.

For EISCAT, the International Polar Year continuous operation came to an end on 29 February 2008, when the ESR was turned off, but the data set continues to draw a considerable amount of interest. It has been suggested that science-driven working groups should be established to address

selected periods within these huge datasets. A new IPY-related ISSI (International Space Science Institute, Berne, Switzerland) working group has started under the leadership of Peter Hoffman, working on bridging the gap in the middle atmosphere. ISSI intends to continue the ground based program and will hold a co-ordinators meeting in May 2009 to plan how this should develop. I expect a new opportunity for EISCAT groups to make proposals in January next year which might well provide a vehicle for the development of working groups.

EISCAT and UNIS, on Svalbard, have established a more formal agreement to develop joint interests on the Island; UNIS has created a full-time academic position to work on radar-related projects.

The success of PFISR, the new US AMISR radar in Alaska, and the data sets collected by the ESR and AMISR during the IPY one-year run, contributed to a new initiative for a high power radar in Antarctica. A workshop (jointly sponsored by the US National Science Foundation's Office of Polar Programs and Upper Atmosphere Facilities section), to explore the scientific case for deploying an incoherent scatter radar in Antarctica, was held in Chicago just prior to the Summer's URSI General Assembly. Participants were invited from all countries thought to have potential interest; I attended as the EISCAT Director, being also a member of the organising committee. Professor Fujii came specially from Japan for the two days of the meeting, and Dr Ian McCrea also attended. Several other members of the EISCAT community, including Dr Kauristie, provided talks, which either I or Anja Strømme (SRI International) gave on their behalf. The workshop revealed considerable interest and support for the project and further work is in progress to prepare formal proposals, budgets, and plans.

Professor Markku Lehtinen and his research team have been considering radar probing of the moon using existing EISCAT capabilities. The first experiments at EISCAT were carried out in December 2008, using separate timing and the first ever EISCAT radar reflectivity maps of the Moon were recorded. We have also received a proposal from Professor Fang, from the National Astronomical Observatories of China, to combine transmissions from EISCAT with reception in China for this purpose. EISCAT will have to improve its time keeping for these initiatives to really work well, but they are certainly very interesting and rather topical in the light of various plans to return humans to the Moon. Our Chinese colleagues have also expressed interest in locating a major antenna for deep-space tracking/communication on Svalbard. The antenna could also be used in conjunction with the ESR and promises to open a number of very interesting new possibilities.

For the first time, the EISCAT Council decided to invite a representative of the staff to attend Council meetings and Peter Bergqvist, from the Kiruna Site, was duly elected as the first Staff Representative, attending the Autumn Council meeting in Kunming, China. Ingemar Häggström, from Headquarters, was also elected as the deputy and attended the special Council meeting in September.

Dr Gudmund Wannberg left EISCAT during the year to return to the Swedish Institute of Space Physics. During his many years with the Association, rising from staff member at the Kiruna Site to Technical and Deputy Director, his scientific, technical, and personal contributions to EISCAT have been immeasurable and done much to shape the Association as it is today. We all wish him well in the future.

There are many challenges in the future, but the EISCAT Scientific Association is in good shape, and has a great and expanding future. I really hope that, with a new Director, a new Council Chair, and newly established plans, all can join forces to ensure that great future really comes to pass. During my tenure as Director, I have tried to move the Association towards a more proactive science role, towards a real and visible position in Europe, and towards a more sustainable financial situation. While I have certainly not achieved everything that I wanted to achieve, and I undoubtedly tried to do too much, I leave the Association stronger than when I began, and that is anyway good. I would like to take this opportunity to congratulate all the staff of EISCAT for your superb work in operating and developing the EISCAT systems to the great state the Association is in today. You have truly carried on the tradition of the early pioneers wonderfully and placed EISCAT at the very front of incoherent scatter radars in the World. The Association, under its next Director, Esa Turunen, has a brilliant future ahead and I look forward to watching its inevitable success over the coming years.

I thank all staff members, past and present, for your dedication and loyalty and wish you all every success in the future!

Prof. Anthony Van Eyken
Director, EISCAT Scientific Association

Scientific highlights of 2008

Ionospheric studies

Climatological features of electron density in the polar ionosphere

In this study, climatological features of the polar F2-region electron density (N_e) are investigated by means of statistical analysis using long-term observations from the EISCAT UHF radar and the EISCAT Svalbard radar (ESR) during periods of quiet to moderate geomagnetic activity. Field-aligned measurements by the radars are used in this study, covering the years 1988–1999 for the UHF radar and 1999–2003 for the ESR. The data are sorted by season (equinox, summer and winter) and solar cycle phase (maximum, minimum, rising and falling). Some novel and interesting results are presented as follows:

1. The well-known winter anomaly is evident during the solar maximum at EISCAT, but it dies out at the latitude of the ESR.

2. The daytime peaks of N_e at EISCAT for all seasons during solar maximum lag about 1–2 h behind those at the ESR, with altitudes about 10–30 km lower.

3. In addition to the daytime peak, it is revealed that there is another peak just before magnetic midnight at the ESR around solar maximum, especially in winter and at equinox (Fig. 1). The daytime ionization peak around magnetic noon observed by the ESR can be attributed to soft particle precipitation in the cusp region, whereas the pre-midnight N_e maximum seems likely to be closely related to substorm events which frequently break out during that time sector, in particular for the winter case.

4. Semiannual variations are found at EISCAT during solar minimum and the falling phase of the solar cycle; at the rising phase, however, the EISCAT observations show no obvious seasonal variations.

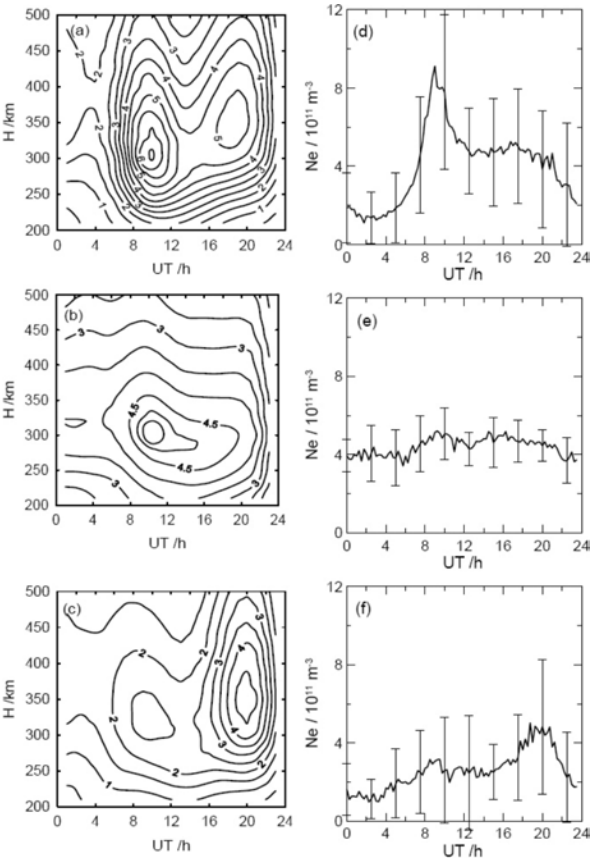

Figure 1: Mean N_e around solar maximum at the ESR site: 2-D distribution vs. UT and H (a, b and c) and diurnal variations at 310 km with error bar (d, e and f). (top panel: equinox; middle panel: summer; bottom panel: winter) (units: 10^{11} m^{-3})

Radar observations are compared with the IRI model. It is found that the predicted results are reasonably consistent with observations as a whole at the EISCAT UHF radar latitude, though the IRI model seems to predict much higher N_e above the F2-peak. The IRI model fails to reproduce seasonal variation at the falling phase, which is obviously shown as a semiannual variation from the radar observations. At higher latitude (around the ESR latitudes), the model fails to reproduce the two-peak structure of N_e distribution vs. UT and height. Detailed comparisons indicate that the predicted results show significant distinctions from the radar measurements, especially at the topside ionosphere and in winter season.

Y. C. Liu, S. Y. Ma, and H. T. Cai, "The background ionospheric profiles at polar cusp latitudes— the ESR observations", Chinese Journal of Polar Research 17(3), 193—202, 2005.

H. T. Cai, et al., "Climatological features of electron density in the polar ionosphere from long-term observations of EISCAT/ESR radar", Annales Geophysicae 25(12), 2561—2569, 2007.

Observations of reverse flow events in the cusp ionosphere with the EISCAT Svalbard Radar

Reverse Flow Events, or RFEs, are narrow channels of intense plasma flow in the opposite direction of the F-region background plasma. They are elongated longitudinally with a width 100–200 km and persisting for 10–20 minutes. RFEs seem to be regulated by Birkeland current arcs in the winter cusp ionosphere above Svalbard. Fig. 2 shows EISCAT Svalbard Radar measurements of an RFE on the left panel—the blue channel of enhanced flow indicated with an arrow. The right panel shows the intensity of the 630.0 nm daytime aurora and illustrates the close correlation of the RFE with auroral precipitation and field aligned currents. The surprising observation of these events was made with the EISCAT Svalbard Radar for the first time in 2001. RFEs seem to be one type of manifestation of the ionospheric signature, among others, of Flux Transfer Events, or FTEs, which are the predominant mechanism of coupling between the solar wind and the magnetosphere and holds the key to many magnetospheric and ionospheric phenomena such as aurora and magnetic storms which continue to be object of intense current research.

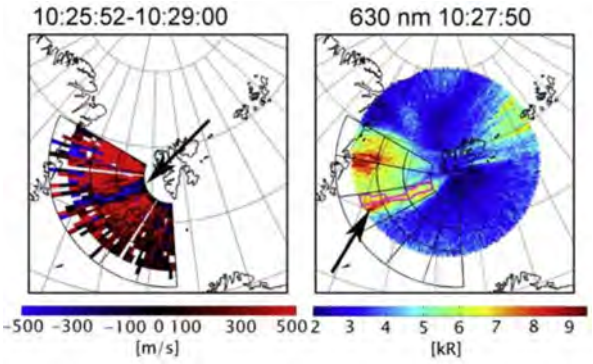

Figure 2: EISCAT Svalbard Radar measurements of an RFE, and the intensity of the 630.0 nm daytime aurora.

Our research of RFEs has established that their onset occurs with the brightening of a discrete arc near the open-closed boundary. The auroral arc is situated exactly at a sharp clockwise flow reversal, consistent with a converging electric field and an upward field-aligned current. One category of RFEs propagates into the polar cap in tandem with poleward moving auroral forms, while another category of RFEs moves with the cusp/cleft boundary. The RFE phenomenon is addressed to a region void of electron precipitation, and in the absence of direct sunlight the E-region conductivity will be very low. Two possible explanations have been proposed by the discoverers of the phenomenon:

1. The RFE channel may be a region where two magnetospheric-ionospheric current loops, forced by independent voltage generators, couple through a poorly conducting ionosphere.

2. The reversed flow channel may be the ionospheric footprint of an inverted V-type coupling region.

Electron beams of <1 keV will not give rise to significant conductivity gradients, and the form of a discontinuity in the magnetospheric electric field will be conserved when mapped down to the ionosphere, although reduced in amplitude. These two explanations may be related in the sense that the boundary discontinuity in the magnetospheric electric field in the first explanation may be the driver for the inverted V in the second one.

J. Moen, et al., "On the relationship between thin Birkeland current arcs and reversed flow channels in the winter cusp/cleft ionosphere", Journal of Geophysical Research 113, A09220, doi:10.1029/2008JA013061, 2008.

Y. Rinne, et al., "On the occurrence of reversed flow events in the cusp ionosphere observed by European Incoherent Scatter (EISCAT) Svalbard radar", Journal of Geophysical Research 112, A10313, doi:10.1029/2007JA012366, 2007.

Comparison of methods to determine ionospheric conductances from ground-based riometer and optical data

Measurements from the UHF radar were used to determine the height-integrated ionospheric conductances in order to verify three methods for estimating the conductances from ground-based optical intensity and radio absorption (riometer) data. These non-radar methods have the advantage that they can provide an imaging capability and so can resolve spatial-temporal ambiguities in ionospheric electrodynamic studies. Figure 3 shows data from 8–9 March 1999. The top row shows selected auroral images at 557.7 nm with two imaging riometer and UHF radar beams overlaid. The second row shows UHF electron density data. The third row shows Hall conductance data measured three different ways. The fourth row shows Pedersen conductance data measured in four different ways. The bottom row shows the Hall-to-Pedersen conductance ratio measured in three different ways. Method S07 consists of "imaging" Hall conductance by imaging riometer. Method K01 consists of "imaging" the characteristic energy of precipitating particles from combined riometer and optical data. Method K98 consists of "imaging" Pedersen conductance from optical data at 557.7 nm. Although simple, the non-radar methods were found to be quite effective, at least for the area close to magnetic zenith, and they can be applied to other locations where incoherent scatter radar is not available to provide a more definitive estimate of ionospheric conductances.

A. Senior, M. J. Kosch, and F. Honary, "Comparison of methods to determine auroral ionospheric conductances using groundbased optical and riometer data", Annales Geophysicae 26(12), 3831—3840, 2008.

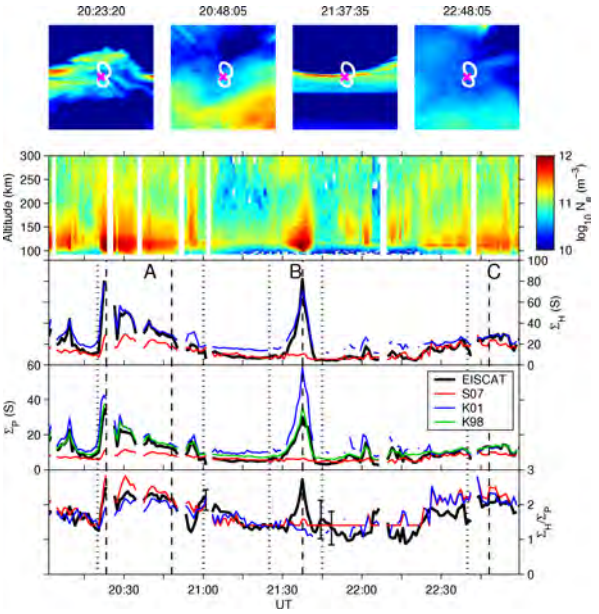

Figure 3: Top row: 557.7 nm images at selected times with two riometer beams overlaid (white ovals) and UHF beam (cross). Second row: electron densities from UHF radar. Third row: Hall conductance. Fourth row: Pedersen conductance. Bottom row: Hall/Pedersen conductance ratio.

Generation of the lower-thermospheric vertical wind estimated with the EISCAT KST radar at high altitudes during periods of moderate geomagnetic disturbance

Lower-thermospheric winds at high latitudes during moderately-disturbed geomagnetic conditions were studied using data obtained with the EISCAT KST UHF radar system on 9–10 September 2004. The vertical neutral-wind speed at 109 km, 114 km, and 120 km heights showed large upward motions in excess of 30 m/s in association with an ionospheric heating event. Large downward speeds in excess of −30 m/s were also observed before and after the heating event. The meridional neutral-wind speed suddenly changed its direction from equatorward to poleward when the heating event began, and then returned equatorward coinciding with a decrease in the heating event. The magnetometer data from northern Scandinavia suggested that the center of the heated region was located about 80 km equatorward of Tromsø. The pressure gradient caused the lower-thermospheric wind to accelerate obliquely upward over Tromsø in the poleward direction. Acceleration of the neutral wind flowing on a vertically tilted isobar produced vertical wind speeds larger by more than two orders of magnitude than previously predicted, but still an order of magnitude smaller than observed speeds. See Fig. 4.

S. Oyama, et al., "Generation of the lower-thermospheric vertical wind estimated with the EISCAT KST radar at high latitudes during periods

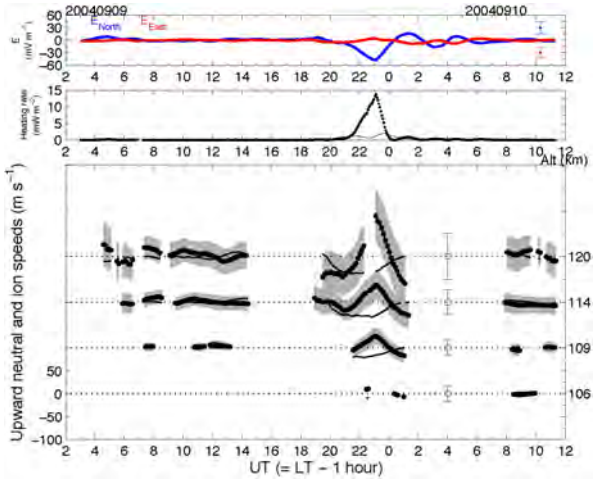

Figure 4: Temporal variations in the electric field (upper panel), the height-integrated passive-energy deposition rate (middle panel; dotted line), and the height-integrated particle heating rate (middle panel; solid line). Bottom panel shows the upward neutral-wind speed (solid curve with dots) and the upward ion speed (solid curve) from 106 to 120 km. The estimated error of vertical neutral-wind speed is shown by gray shading above and below the line. The vertical bar with a square at each height is the mean error value $\pm 1\sigma$ of the vertical neutral-wind speed from 19 to 2 UT.

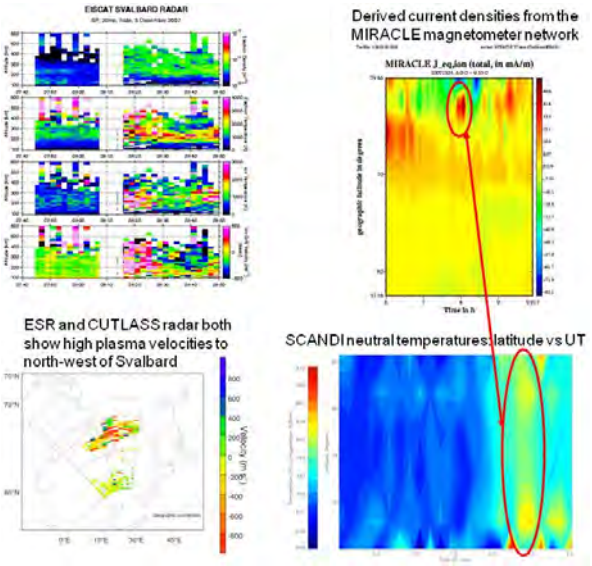

Figure 5: Observations of highly localised ion-neutral coupling effects, both spatial and temporal, using a network of instruments over Svalbard on 5th December 2007. Top left panel: ESR data. Top right panel: Derived current densities from the MIRACLE magnetometer network. Bottom left panel: CUTLASS SuperDARN radar velocity data. Bottom right panel: Thermospheric neutral temperature.

of moderate geomagnetic disturbance", Annales Geophysicae 26(6), 1491—1505, 2008.

Ionosphere-thermosphere meso-scale coupling studies

Thermospheric response to ionospheric forcing is traditionally contemplated in terms of large spatial scales of several hundred kilometres and a few hours. Co-located ion-neutral coupling studies using the ESR and University College London all-sky Scanning Doppler Imager (SCANDI) as well as the mainland UHF radar and tri-static Fabry-Perot interferometers (FPI) have shown a far more dynamic and responsive thermosphere than expected when measured at higher spatial and temporal resolution. The importance of these meso-scale coupling experiments is that the observations of the ionosphere and thermosphere are made independently, are of the same volume of the atmosphere, and are unique to EISCAT.

SCANDI observes the 630 nm optical emission, which peaks at ∼240 km altitude, giving measurements of the neutral winds and temperatures with ∼180 km resolution in a field of view of ∼600 km radius every ∼8 minutes. Figure 5 shows an example of a highly localised heating event, both temporally and spatially. On the night of the 5–6 December 2007 there occurred a brief northward spike in the B_z component of the IMF observed by the ACE satellite, which corresponded to a highly localised surge in plasma velocities lasting ∼20 minutes over a region of ∼300 km in latitude to the north-west of Svalbard. The timing of the velocity surge was seen in the ESR line-of-sight plasma velocities, and the spatial extent was seen in the CUTLASS fan plot, as well as the plot of equivalent currents from the MIRACLE magnetometer chain. The SCANDI winds and temperatures showed an almost immediate response to this heating effect. The magnitude of the winds and intensities seen in the north-west zones alone of the SCANDI FOV rapidly increased by nearly 200 m/s and a factor of 4, respectively, over a half hour period. These high values remained for nearly half an hour before returning to previous levels. The neutral temperatures rose quickly too, by a maximum of 100 K, but then declined over the next 2 hours. In contrast to the localised increase in winds and intensities, the temperature rise spread to the whole field of view.

A detailed study of three periods of ionospheric heating, observed by the ESR and SCANDI on the night of 15-16 March 2007, shows how E-region Joule heating increased the upper thermospheric temperature more than F-region heating, but the biggest temperature increase came from frictional heating due to large ion and neutral velocities.

The peak emission altitude of the 630 nm airglow/aurora is vitally important for FPI observations of thermospheric parameters since it determines where the emitting volume is. From ESR-SCANDI and UHF-FPI campaigns in January and February 2008, respectively, the ESR/UHF radar electron densities are used to model the height profile of the 630 nm emission intensity. The model also gives the ion densities of the three major species: O^+, NO^+ and O_2^+, which are being used to test the usual assumption of 100% O^+ used for standard analysis of EISCAT radar data. There are several examples of when the apparent ion temperature measured by the EISCAT is less than the SCANDI/FPI neutral temperature, which is physically unfeasible since the ions sit in a bath of neutral particles. Whether this occurs during periods of upwelling, when molecular species are brought to these altitudes, or when the plasma velocity is no longer an isotropic Maxwellian distribution, is under investigation.

The contribution of the thermosphere to the three-dimensional behaviour of the ionosphere has also been addressed. Current modelling and data analysis techniques work in one dimension (e.g. field-aligned, along a radar beam) or in two dimensions (e.g. horizontally, over a network of magnetometers). It is suggested that it is time to move to a full 3D representation. Three major new themes have been identified: ionospheric induction, current closure and the thermospheric contribution.

E. M. Griffin, et al., "Upper thermospheric neutral wind and temperature measurements from an extended spatial field", Annales Geophysicae 26(9), 2649-–2655, 2008.

O. Amm, et al., "Towards understanding the electrodynamics of the 3-dimensional high-latitude ionosphere: Present and future", Annales Geophysicae 26(12), 3913—3932, 2008.

Comparison of lower thermosphere electron density measured with EISCAT and modelled with HAMMONIA—first results

The Hamburg Model of the Neutral and Ionized Atmosphere (HAMMONIA) is a general circulation and chemistry model that treats atmospheric dynamics, radiation, and chemistry interactively for the height range from the Earth's surface to the thermosphere (approximately 250 km). It is based on version 5 of the ECHAM atmospheric general circulation model of the Max Planck Institute for Meteorology in Hamburg. It is extended for important radiative and dynamical processes of the upper atmosphere. To study the effects of precipitating energetic particles a couple of processes have been modified or added to HAMMONIA. These modifications are described in the following.

The chemistry module includes 214 reactions among 49 neutral and 5 ion (O^+, O_2^+, N^+, N_2^+, NO^+) species, and electrons. The formation of ions due to photoionization caused by extreme ultraviolet and shorter wavelengths is calculated using a parametrization of Solomon and Qian [JGR (2005)]. This parametrization also considers ionization by secondary electrons. Additionally, ions are produced by the impact of precipitating energetic particles. HAMMONIA uses three-dimensional sets of time dependent ionization rates by precipitating protons, electrons, and alpha particles. These ion pair production rates are computed by the Atmospheric Ionization Module Osnabrück (AIMOS). They are based on multi-satellite measurements. In HAMMONIA above 1×10^{-3} hPa the ionization rates are explicitly used to compute reaction rates of ionization, dissociation, and excitation of N, N_2, O, and O_2. Below 1×10^{-3} hPa, where atmospheric ion chemistry is more complex, parametrizations of Porter et al. [JCP (1976)] and Solomon et al. [PSS (1981)] are used to produce N(^4S), N(^2D), and NO_x. HAMMONIA considers heating by a series of exothermic chemical reactions involving ions and excited species. Cooling from nitric oxide at 5.3 μm is calculated by using a parametrization of Kockarts [GRL (1980)]. Joule heating and ion drag are calculated following the parameterization of Zhu et al. [AG (2005)] based on the ionospheric convection pattern which is presented by Heelis et al. [JGR (1982)].

Figure 6 shows the comparison of electron density profiles which are calculated using the HAM-

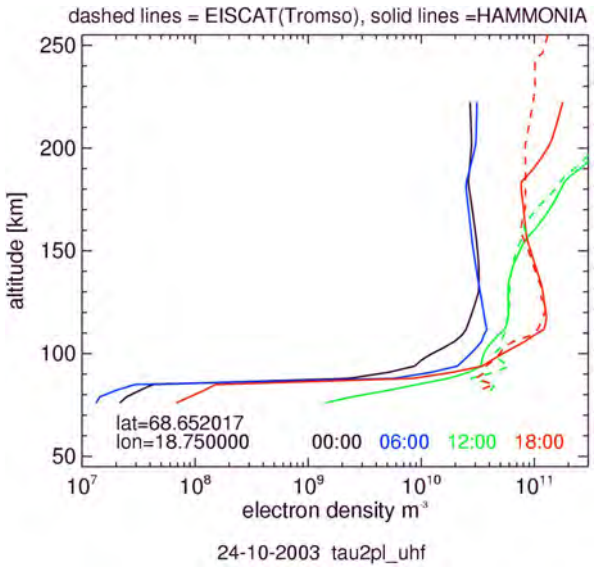

Figure 6: Height profiles of electron densities calculated using the model HAMMONIA compared to EISCAT UHF measurements. The two-hourly means were calculated at a grid point next to the EISCAT UHF site near Kiruna for Oct. 24 and Nov. 19, 2003.

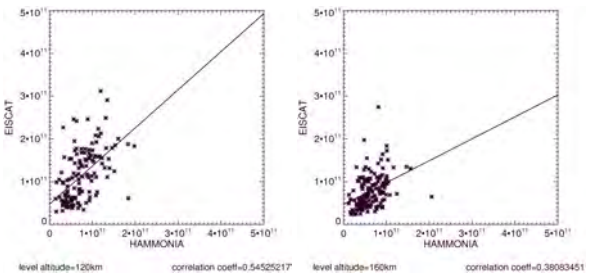

Figure 7: Direct comparison of two-hourly means of electron density estimates derived from the HAMMONIA model and from EISCAT UHF radar measurement for the period Oct. 20 till Nov. 20, 2003. Left panel: Density at 120 km; Right panel: Density at 160 km.

MONIA model and which are derived from EISCAT UHF radar measurements. The two-hourly height profiles from the model calculation of the electron densities are shown for four time periods on a day where simultaneous EISCAT UHF radar measurements are available for two periods. The electron densities derived from the HAMMONIA model are essentially determined by the ionization rates which are derived from AIMOS with a time resolution of two hours. This time resolution for a comparison between model and experiment is reasonable because of short period fluctuations in the experimental data.

Figure 7 shows the direct comparison of electron densities derived from the HAMMONIA model and from EISCAT UHF radar measurements. Two-hourly averages are prepared for the time period between October 20th and November 20th, 2003. The first results are shown for two heights (120 and 160 km) and the agreement to EISCAT measurements is obvious for this example.

H. Schmidt, et al., "The HAMMONIA chemistry climate model: Sensitivity of the mesopause region to the 11-year solar cycle and CO_2 doublings", Journal of Climate 19(16), 3903–3931, 2006.

J. M. Wissing and M.-B. Kallenrode, "Atmospheric ionization module Osnabrück (AIMOS): A 3-d model to determine atmospheric ionization by energetic charged particles from different populations", Journal of Geophysical Research, 114(A6), A06104, doi:10.1029/2008JA013884, 2009.

The influence of dayside ionospheric plasma on the nightside plasma distribution

Studies of large-scale ionospheric footprints of solar wind–magnetosphere coupling processes have been carried out with EISCAT data complementing radio-tomography observations. These studies concentrate on polar patches, i.e. plasma enhancements that originate on the dayside in the sunlit ionosphere that are transported anti-sunward across the polar cap into the nightside sector. The patches have electron densities of at least twice the background level and horizontal spatial extents of at least 100 km. Modelling studies show that the transport of plasma across the polar cap is expected to maximise when Europe is on the nightside, due to the offset between the geomagnetic and geographic reference frames.

The transport of patches in the convective flow across the polar cap from dayside to nightside under conditions of IMF B_z negative is well established. However, the more complicated high-latitude plasma convection patterns for IMF B_z positive means that the influence of transport on the nightside plasma distribution under this condition is not so well understood. Using multi-instrument observations from the ESR, the SuperDARN radar network and radio-tomography, it is revealed that plasma flowing from the dayside can also play a significant role in the nightside ionosphere under IMF B_z positive. Figure 8 shows, for IMF B_y negative, two regions of cold, long-lived plasma in the winter nighttime ionosphere that

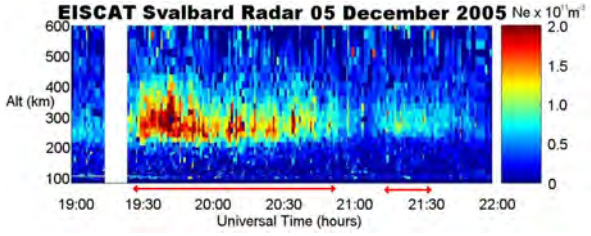

Figure 8: Electron densities observed by the ESR 42 m radar. Two regions of enhanced densities are observed in the nightside sector (at approximately 1930-2050 UT and 2115-2130 UT respectively) separated by a region of lower densities.

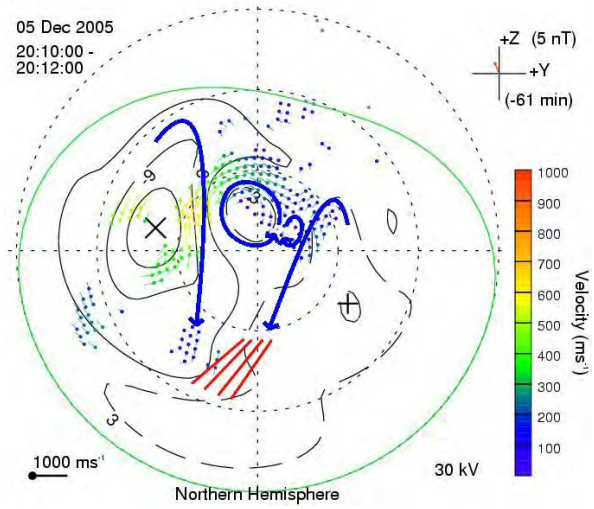

Figure 9: SuperDARN flow measurements and electric potential map confirming the presence of a pair of lobe cells that were essentially blocking direct antisunward cross polar flow from the dayside to the nightside, thus causing a region of lower densities separating the two nightside enhancements.

were extended in MLT and separated by a region of lower densities near magnetic midnight. The earlier enhancement between about 1930 UT and 2050 UT was attributed to dayside plasma, which had originated near magnetic noon, whilst the later feature between about 2115 UT and 2130 UT was believed to have originated in the magnetic morning sector. Figure 9 shows that the region of lower densities separating the two enhancements was a consequence of a pair of lobe cells essentially blocking the direct antisunward cross polar flow from the dayside. The observations were reinforced by simulations of flux-tube transport and plasma decay.

Formation and maintenance of the main, or mid-latitude, ionisation trough in the post-midnight sector remain open questions. Radio-tomography observations in Scandinavia and the UK revealed a persistent large-scale electron density enhancement in the post magnetic midnight sector, forming the poleward wall of the main trough. Simultaneous observations by the ESR ruled out in situ soft-particle precipitation as the main source of the higher densities, whilst the SuperDARN plasma flow and electric potential patterns placed the feature in the dawn cell of the high-latitude convection. It was inferred that the plasma had originated as photoionisation on the dayside and had convected over the polar cap and into the nightside. These multi instrument observations provide essential ground truth for modelling investigations where electric potential patterns from the SuperDARN radar network are used as input to the Coupled Thermosphere-Ionosphere-Plasmasphere model (CTIP). The SuperDARN patterns improve the modelling of the high-latitude ionospheric plasma distribution under IMF B_z negative, and enables modelling under IMF B_z positive using a convection pattern appropriate for the condition. In the case of IMF B_z negative both the model and the observations reveal a tongue-of-ionisation, with good agreement in its electron density and location. Under B_z positive the model reproduces a spatial plasma distribution akin to that observed, with the plasma being drawn by the convective flow in a tongue-of-ionisation around the periphery of the polar cap.

The influence of geomagnetic substorm activity on the latitudinal spatial distribution of polar patches in the nightside sector has also been studied. The ESR radar and the radio-tomography receiver chain observed the remnants of the patches in the nightside ionosphere as they traversed from the polar region to auroral latitudes. During substorm expansion the patches were separated by some 5° latitude, but this was reduced to some 2° when the activity had subsided. The different patch separations were attributed to the expansion and contraction of the high-latitude plasma convection pattern on the nightside in response to the substorm activity.

A. G. Wood, et al., "Multi-instrument observations of nightside plasma patches under conditions of IMF B_z positive", Annales Geophysicae 26(8), 2203—2216, 2008.

H. R. Middleton, et al., "The role of the tongue-of-ionisation in the formation of the poleward wall of the main trough in the European post-midnight sector", Journal of Geophysical Research 113, A02306, doi:10.1029/2007JA012631, 2008.

A. G. Wood, "Multi-instrument studies of polar cap patches in the high-latitude nightside ionosphere", PhD thesis, University of Wales, 2008.

Strong electron heating in the E Region

Observations by the EISCAT Svalbard radar show that electron temperatures T_e in the cusp electrojet reach up to about 4000 K. The heat is tapped and converted from plasma convection in the near Earth space by a Pedersen current that is carried by electrons due to the presence of irregularities and their demagnetising effect. The heat is transfered to the neutral gas by collisions. In order to enhance T_e to such high temperatures the maximally possible dissipation at 50% demagnetisation must nearly be reached. The effective Pedersen conductances are found to be enhanced by up to 60% compared to classical values. Conductivities and conductances respond significantly to variations of the electric field strength E, and "Ohm's law" for the ionosphere becomes non-linear for large E. See Fig. 10.

S. C. Buchert, et al., "The Pedersen current carried by electrons: A non-linear response of the ionosphere to magnetospheric forcing", Annales Geophysicae 26(9), 2837–2844, 2008.

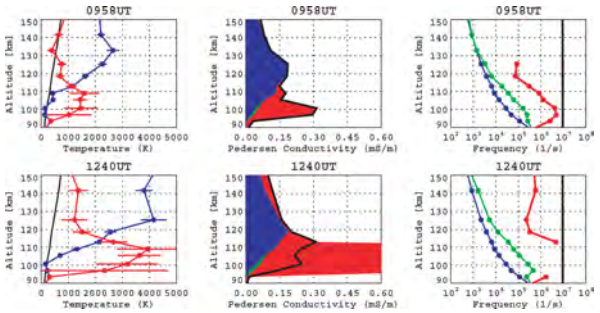

Figure 10: Each column of plots shows from left to right altitude profiles of temperatures, Pedersen conductivity, and collision frequencies, respectively. In the temperature profiles T_e is plotted in red, T_i in blue, and T_n as black line. In the conductivity profiles the blue area shows the classical Pedersen conductivity calculated according to Brekke and Hall (1988), the (mostly hardly visible) green area the increase of σ_P due to enhanced T_e, and the red area the additional contribution from an anomalous σ_P^*. The black line cuts through the red area whenever no corresponding real anomalous ν_* could be calculated and shows the conductivity value corresponding to $\nu_* = \Omega_e$ instead. In the frequency profiles ν_{en} is plotted in blue, ν_{en} corrected for the observed T_e in green, ν_* in red, and Ω_e as a black line. The upper row shows a time of modest electron heating, the lower row one of very extreme heating.

Auroral studies

Electric fields and currents of high-latitude auroral arcs

Post-noon (15–16 MLT) poleward moving auroral arcs were observed in January 2008 over Svalbard during slightly negative IMF B_z and the IMF B_y gradually changing from near-zero to about -3 nT. The steerable 32-m antenna of the EISCAT radar was directed at an elevation angle of 45°, to the north-west at about 45° to geomagnetic west, allowing for measurement of azimuthal (along east-west) plasma flow in a range of latitudes. On the basis of this radar configuration, a new method has been developed and applied for calculating of the field-aligned currents in the vicinity of the arcs. The arcs were located in the region of post-noon convection reversal and background upward FAC of about 1 μA/m^2 in magnitude. The optical arcs were of the order of 30–40 km wide and coincided with peaks of upward FAC. The return downward FAC and southward electric field was observed poleward of the arcs. Equatorward of the arcs, secondary weaker arcs were detected, so that

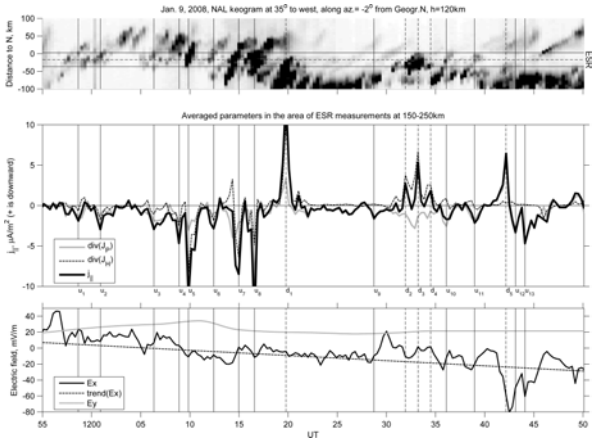

Figure 11: Top panel: Keogram from Ny Ålesund. Middle panel: Field-aligned currents calculated in the area indicated as "ES" in the top panel. Bottom panel: The electric field x- and y-components (across and along the arcs, respectively) against time; the values of electric field x-component are averaged over the region where the field-aligned currents were calculated.

the post-noon arcs appear to have a double structure. These features are surprisingly similar to the electric field and current patterns of morning Sun-aligned arcs reported earlier by Kozlovsky et al. [JGR, 2007]. We suggest that the double arc structure can be explained by the non-linear ionospheric feedback that results in splitting of the elongated magnetospheric plasma structures associated with the arcs. See Fig. 11.

A. Kozlovsky, T. Turunen, and S. Massetti, "Field-aligned currents of postnoon auroral arcs", Journal of Geophysical Research 114, A03301, doi:10.1029/2008JA013666, 2009.

Auroral imaging in the 731.9 nm O^+ line

Simultaneous observations were made of dynamic aurora during substorm activity on 26 January 2006 with three high spatial and temporal resolution instruments: the ASK (Auroral Structure and Kinetics) instrument, the SIF (Spectrographic Imaging Facility) and the ESR (EISCAT Svalbard Radar), all located on Svalbard (78°N, 16.2°E). One of the narrow field of view ASK cameras is designed to detect O^+ ion emission at 731.9 nm. From the spectrographic data we have been able to determine the amount of contaminating N_2 and OH emission detected in the same filter. This is of great importance to further studies using the ASK instrument, when the O^+ ion emission will be used to detect flows and afterglows in active aurora. The ratio of O^+ to N_2 emission is dependent on the energy spectra of electron precipitation, and was found to be related to changes in the morphology of the small-scale aurora. The ESR measured height profiles of electron densities, which allowed estimates to be made of the energy spectrum of the precipitation during the events studied with optical data from ASK and SIF. It was found that the higher energy precipitation corresponded to discrete and dynamic features, including curls, and low energy precipitation corresponded to auroral signatures that were dominated by rays. The evolution of these changes on time scales of seconds is of importance to theories of auroral acceleration mechanisms. See Fig. 12.

H. Dahlgren, et al., "Using spectral characteristics to interpret auroral imaging in the 731.9 nm O^++ line", Annales Geophysicae 26(7), 1905–1917, 2008.

Poleward boundary intensifications of the auroral oval

In this study, the two beams of the EISCAT VHF radar were used to estimate the polar cap boundary location and orientation. In addition, the reconnection electric field was calculated by using the measurements of plasma flow across the boundary. Optical observations were provided by the Polar satellite UV Imager. The study showed quantitatively, for the first time to our knowledge, that intensifications in the local reconnection electric field have one-to-one correlation with the appearance of auroral poleward boundary intensifications (PBIs). PBIs are transient nightside geomagnetic disturbances, with a localized auroral signature that appear at the poleward boundary of the auroral oval, and can then extend equatorward inside the auroral oval. The results suggest that PBIs are a consequence of longitudinally localized magnetic flux closure in the magnetotail, lasting for 5–12 min. See Fig. 13

T. Pitkänen, et al., "Reconnection electric field estimates and dynamics of high-latitude boundaries during a substorm", Annales Geophysicae 27(5), 2157—2171, 2009.

Small scale auroral studies

The ASK (Auroral Structure and Kinetics) optical instrument was installed close to the UHF radar for the 2006–2007 winter season. The events shown in Fig. 14 are from a night of active aurora on 22 October 2006. The top panel is the

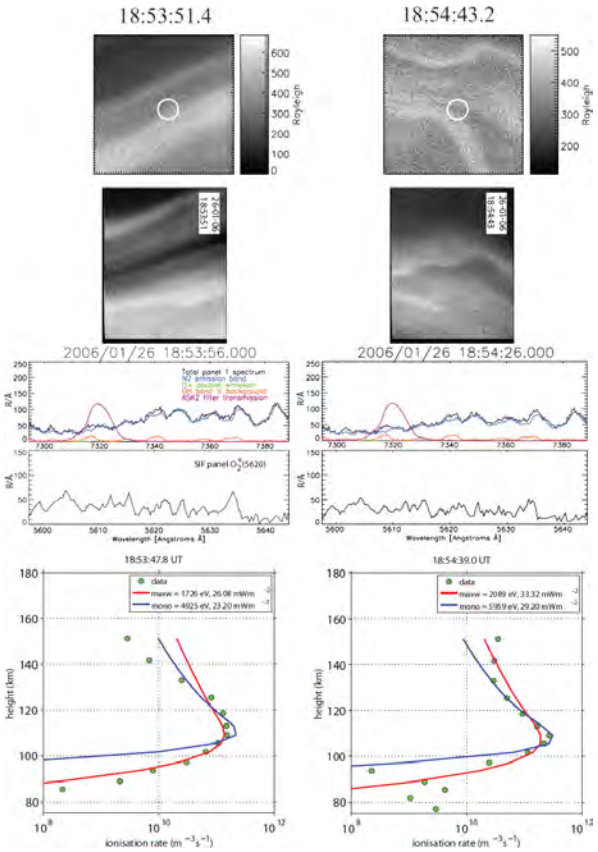

Figure 12: Optical and electron density data from 18:53 UT. The top row shows ASK3 images, the second row SIF video camera images, the third row ESR electron density profiles, and the fourth row SIF spectra. In the video camera images the position of the spectrographic slit is plotted, and the part with the mosaic filter letting through emissions at 732.0 nm is marked in red.

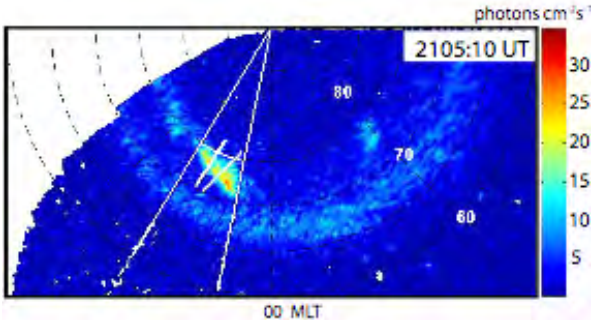

Figure 13: Polar UVI image of aurora in the night sector including the two VHF beams (short white lines) measuring the PBI structure (yellow and orange).

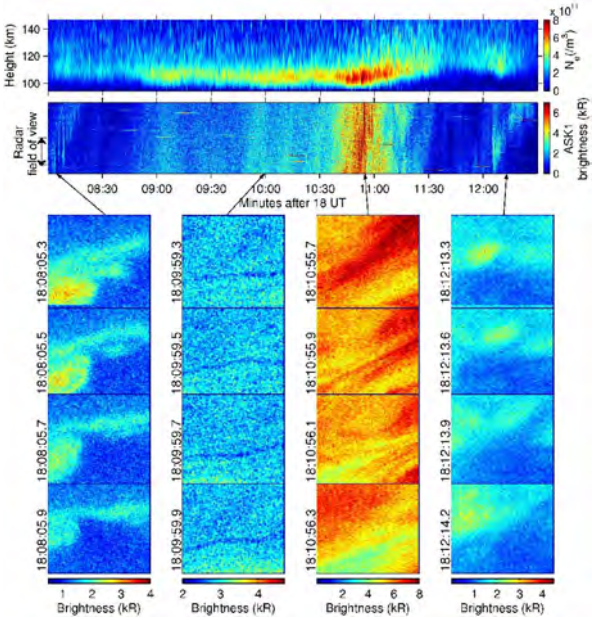

Figure 14: Overview of the UHF radar and ASK optical data between 18:08:00 and 18:12:30 UT on 22 October 2006, showing electron density (top panel), emissions from ASK1 (second panel), and selected images during 1 s intervals as marked with arrows (lower panels).

measured electron density in the E-region between 95 and 150 km. The second panel is a time series of slices taken across the images from ASK1. The slices are made from a central meridian cut, i.e. 3° north-south aligned. The approximate position and size of the radar field-of-view is marked on the left-hand axis. Below this panel are sample ASK1 images from four selected intervals, using false colour to demonstrate the small scale variations more clearly. In each interval there is a time sequence lasting less than one second. The first selected interval shows the passage of a curling thin arc across the field of view. Five separate curls move from right to left, folding and unfolding in the process. The second interval shows a period of diffuse aurora with very narrow (<150 m) dark lanes moving through the field of view. The third interval is at the peak of the brightest event, when the camera measured swirling, narrow filaments. The final interval follows a time of lower activity, when more diffuse curl-like patches move across the field of view.

Radar profiles of electron density have been used as input to the auroral model. Estimates of the energy and flux of precipitation are obtained, making it possible to validate the model by comparing measured emission rates from the

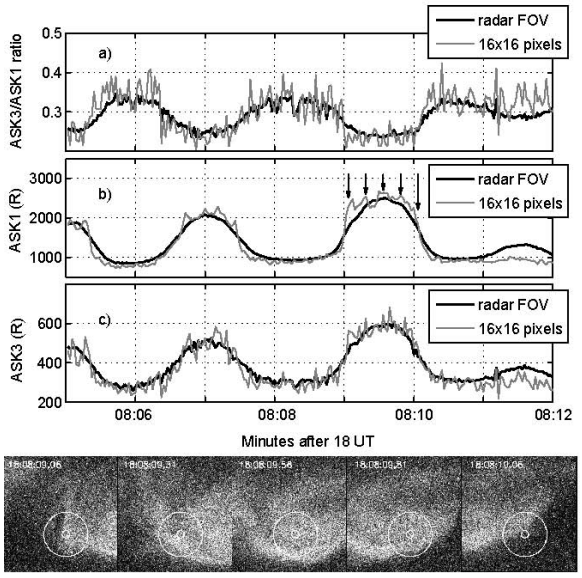

Figure 15: (a) Measured OI/N_2 ratio, (b) brightness of ASK1, and (c) ASK3, from 18:08:05 to 18:08:14 UT, at two spatial resolutions: the field of view of the UHF radar (black) and 16×16 pixels in the magnetic zenith (grey). The bottom panel shows images 250 ms apart starting at 18:08:09 UT as marked in (b).

ASK instrument with modelled values. The ratio of emissions within the ASK field of view can then be used to give estimates of energies at unprecedented resolution in time and space. As a result of this excellent fit, the model was then used to obtain the emission brightness for the three ASK imagers in the radar field of view. The results made a very good fit such that the ratio of ASK3/ASK1 (OI/N_2) was then used to estimate the changes in energy within the auroral structures.

The top panel of Fig. 15 is a short time series of the measured OI/N_2 brightness ratio at the highest time resolution of 32 fps during the passage of the sequence of auroral curls shown in Fig. 14. These have been integrated over an area of about 200×200 m at 100 km height in the magnetic zenith (grey curve), which is still larger than the smallest features observed. For comparison the changes within the field of view of the radar are included (black curve). The relative sizes of these fields of view are shown in the images below. The second and third panels are the brightness of both ASK1 and ASK3 during the same sequence, and at the same spatial resolution. The fourth curl is not measured in the zenith, but it is contributing to the signal in the wider integration region.

Examination of the images at this time resolution shows that the fluctuations in the emissions within each curl are significant. The images in the bottom row of Fig. 15 show the passage of the third curl, over 1 second. The times of the images are marked with arrows on the second panel, which is the N_2 brightness, and thus directly related to the flux. The images are separated by 250 ms showing the changes in intensity within the thin filament as it winds and unwinds. The first arrow corresponds to the abrupt change as the narrow feature enters the small field of view. At the time of the second arrow, a sudden brightening of the narrow filament has moved through the smaller field of view. Following this the narrow gap between the curling filaments is measured. At the time of the final arrow most of the curl feature has moved out of the selected region. The observed OI/N_2 ratio varies between 0.2 in the bright filaments and 0.4 in the region outside the curl. These values correspond to peak energies in the region of 20 keV within the curl and energies of 5-–10 keV outside the bright feature. Values of flux are estimated from the N_2 brightness in the smaller zenith field of view. As the curl enters this region the flux increases from approximately 3 to 7 mW/m^2.

B. S. Lanchester, et al., "Simultaneous imaging of aurora on small scale in OI (777.4 nm) and $N_2$1P to estimate energy and flux of precipitation", Annales Geophysicae 27(7), 2881–2891, 2009.

Studies of polar mesospheric summer echoes

Microphysical parameters of mesospheric ice clouds derived from multiple frequency radar soundings

Simultaneous and common volume measurements of polar mesosphere summer echoes (PMSE) were conducted in June 2006 at two frequencies (53.5 and 500 MHz). The SOUSY Svalbard Radar (SSR) and the EISCAT Svalbard Radar (ESR) are collocated near Longyearbyen on the island of Spitsbergen (78°N, 16°E) with Bragg wavelengths of 2.8 m and 0.3 m, respectively. The wavelengths are well separated and allow a comparison of PMSE occurrence rates, turbulence parameters, and the volume reflectivities. The microphysics of the ice clouds observed near mesopause altitudes is studied under the assumption of the theory that turbulence and large Schmidt numbers are necessary for the existence of these strong radar echoes.

During the period of the experiment PMSE was observed for 94.5% of the observation time by the SSR at 2.8 m Bragg wavelength and for only 16% by the ESR with a Bragg wavelength of 0.3 m. Additionally, the height range is larger at 2.8 m (80—92 km) than at 0.3 m (81—88 km) where PMSE occur. The analysis of the spectral width has shown that this parameter is larger if echoes above 85 km were observed at both wavelengths simultaneously than only at 2.8 m. The spectral width of the radar measurements can be converted into turbulence energy dissipation rates, 5-–200 mW/kg, which are in the same order of magnitude as estimated from in-situ rocket-borne turbulence measurements.

The returned echo strength of both radars can be compared quantitatively if the absolute volume reflectivity η is determined from noise calibration in the case of the ESR as well as a delay line and noise calibration applied at the SSR. Figure 16 demonstrates the estimated values of η for the 0.3 m ESR echoes and for the 2.8 m SSR echoes, respectively. The large dynamical range is caused by the high geophysical variability of PMSE demanding that quantitative comparisons of volume reflectivities are only reliable on the basis of simultaneous and common volume measurements. Figure 17 displays the volume reflectivity $\eta(k)$ calculated for different Schmidt numbers Sc which correspond to different particle radii. The two vertical bars indicate the Bragg wavenumbers of the SSR ($k = 2.24$ m^{-1}) and the ESR ($k = 20.93$ m^{-1}), respectively. If the Schmidt number is large the ratio between η_{SSR} and η_{ESR} should be a constant value since $\eta(k) \propto k^{-3}$ holds. In this case the Schmidt number falls into the viscous-convective subrange. In the case where the Schmidt number is not very large the reflectivity η_{SSR} follows the k^{-3} dependence but η_{ESR} decreases exponentially. In consequence, the ratio $\eta_{\mathrm{SSR}}/\eta_{\mathrm{ESR}}$ should be larger than the minimum $(k_{\mathrm{SSR}}/k_{\mathrm{ESR}})^3 = 816$ in those cases. Indeed, 94% of the observations satisfy this criteria. Taking into account the corresponding accuracies of volume reflectivity as well as the small radar volumes this is considered as good agreement with theory. The results confirm that calibrated radar measurements of PMSE at two well-separated Bragg wavelengths is a very efficient tool to study the microphysics of mesospheric ice clouds and related questions such as solar induced variations as well as long term trends.

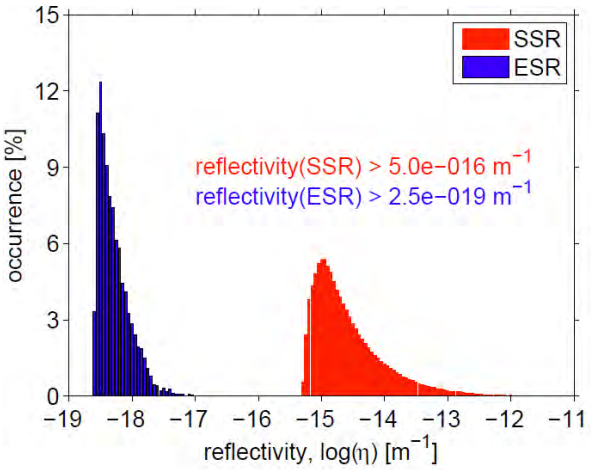

Figure 16: Histograms of absolute volume reflectivities at 500 MHz and 53.5 MHz derived from the ESR (blue) and SSR (red) observations in June 2006. Minimum detectable values for both radars are included in the figure.

Q. Li, et al., "Microphysical parameters of mesospheric ice clouds derived from calibrated observations of polar mesosphere summer echoes at Bragg wavelengths of 2.8 m and 30 cm", Journal of Geophysical Research 115, D00I13, doi:10.1029/2009JD012271, 2010.

Spectral characteristics of PMSE observed at VHF and UHF frequencies

The nature of PMSE observed at VHF and UHF frequencies is investigated by analysing the shape of the autocorrelation function (ACF) which is the Fourier transform of the Doppler spectrum. The spectral shape of the radar returns received by incoherent scatter radars (ISR) can be divided into three cases. The Doppler spectrum of pure incoherent scatter in the D-region exhibits a Lorentzian shape where the spectral area is proportional to the electron density and the width is determined by the ion diffusivity. The Doppler spectrum of coherent scattering from mesospheric altitudes, like PMSE, has a Gaussian shape because it is characteristic for the velocity distribution due to turbulent motion of the scatterers. In this case the incoherent part is hidden under the coherent component. The third case occurs in the presence of charged aerosol particles which is a superposition of two Lorentzian spectra due to positive ions and heavier charged dust particles. A simple method is introduced to quantify these different spectral shapes with only one parameter from a generalized exponential fit to the ACF: i.e. $ACF(\tau) = ACF_{\tau=0} \cdot \exp\left[-(\tau/\tau_{\mathrm{e}})^n\right]$, where ACF is the magnitude of the autocorrelation function, τ the time

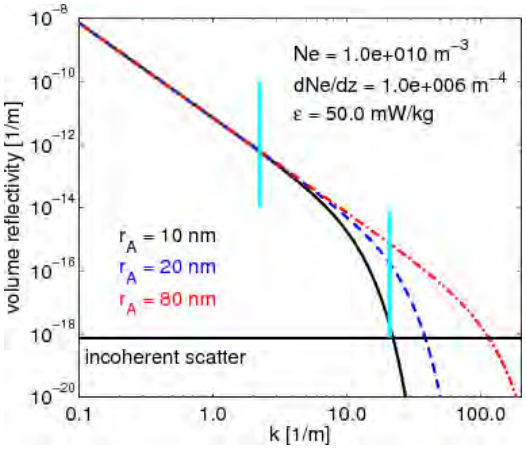

Figure 17: Calculated volume reflectivity for turbulent backscatter for a turbulent energy dissipation rate of 0.1 W/kg. The lines were calculated for Schmidt numbers $Sc = 650, 2600, 41600$ corresponding to radii $r_A = 10, 20, 80$ nm, respectively. The two vertical bars indicate the Bragg wavelength of the SSR (left) and the ESR (right). The black horizontal line indicates the volume reflectivity due to incoherent scatter for an electron density of 1×10^{10} m^{-3} for comparison.

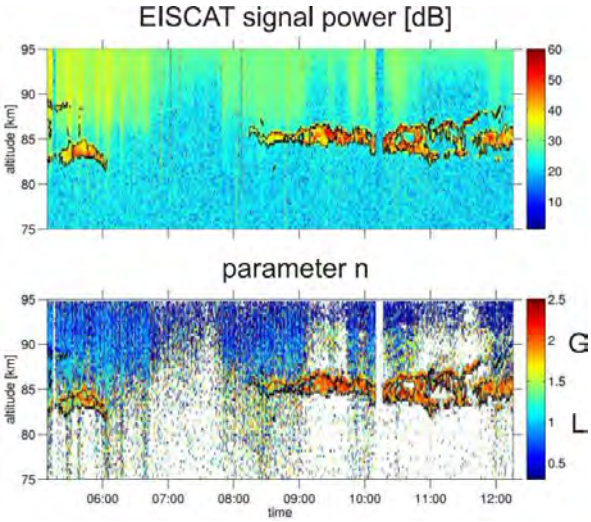

Figure 18: EISCAT VHF measurements of PMSE on July 1st, 2003 using the arc-dlayer experiment. Upper panel: signal power; lower panel: parameter n derived from the measured ACF.

lag at which the ACF is evaluated and τ_e the correlation time of the ACF. The exponent describes the shape of the ACF where $n = 2$ corresponds to a Gaussian and $n = 1$ to a Lorentzian shape, respectively, whereas $n < 1$ reflects the presence of charged dust particles. This behavior holds for altitudes between 70 and 90 km.

Figure 18 shows the EISCAT VHF observation during a PMSE event during polar summer 2003. The upper panel displays the signal power and the lower panel the parameter n. The blue color in the lower panel corresponds to pure IS where the ACF has a Lorentzian shape which holds for areas outside the PMSE layer. Inside the PMSE layer the spectra are Gaussian as shown by the red color. A statistical analysis of 86 h of PMSE observations is shown in Fig. 19. It is clearly seen that the parameter $n = 1$ outside the PMSE where IS dominates the spectrum and inside the PMSE the spectrum is identified to have a more Gaussian shape. This supports the point that PMSE originate from scattering at coherent structures.

Figure 20 shows two cases of EISCAT measurements (ACF and spectra). During both cases PMSE was observed by the VHF radar. The top row shows spectra where a Gaussian type was found for the VHF and the UHF radar with nearly the same spectral width indicating that the scattering is determined by the energy dissipation

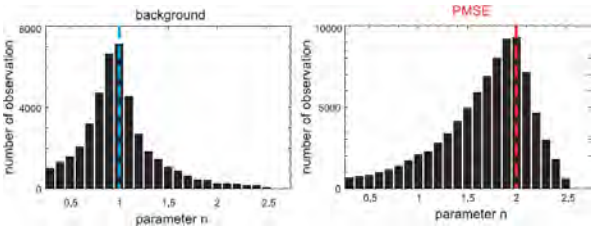

Figure 19: Statistical analysis of 86 h of EISCAT PMSE observations. Left: outside the PMSE layer (dominated by $n = 1$) and inside PMSE (dominated by $n \simeq 2$).

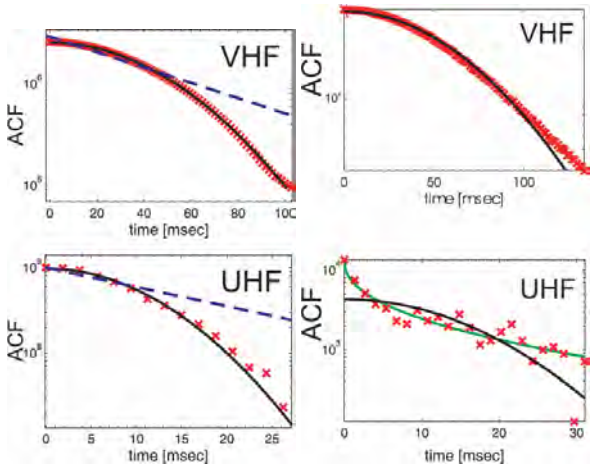

Figure 20: PMSE observation with EISCAT VHF (top) and UHF (bottom) radars. Red crosses mark the magnitudes of the the ACFs of the collected time series, the black line a Gaussian fit and the blue dashed line a Lorentzian fit. Left panels: Coherent scatter in the vicinity of PMSE for VHF and UHF radar. Right panels: Coherent scatter for VHF but incoherent modified by dust for the UHF.

due to turbulence. This confirms that turbulence-induced electron density irregularities influence the spectral shape of the signal received by the UHF radar. Another case is shown in the bottom row of Fig. 20 where the turbulence-induced fluctuations do not influence the scattering at UHF frequencies. Here, the spectrum shows the superposition of two Lorentzian lines as described above, i.e. due to the existence of heavy charged ice particles, as present in PMSE, the spectrum also contain a narrow particle line in addition to the ion line.

The shape of the ACF yields information about the scattering entities contributing to the signal. Once the spectral shape is determined further analyses can be chosen. In the case where the UHF spectra are not influenced by coherent structures of turbulence the particle radii can be determined.

I. Strelnikova and M. Rapp, "Studies of polar mesosphere summer echoes with the EISCAT VHF and UHF radars: Information contained in the spectral shape", Advances in Space Research 45(2), 247–259, doi:10.1016/j.asr.2009.09.007, 2010.

I. Strelnikova, et al., "Meteor smoke particle properties derived from Arecibo incoherent scatter radar observations", Geophysical Research Letters 34(15), L15815, doi:10.1029/2007GL030635, 2007.

Recent investigations of Polar Mesospheric Summer Echoes subject to RF Modification with the MORRO and the EISCAT Radars

An investigation of Polar Mesospheric Summer Echoes (PMSE) subject to RF modification has been carried out with the MST MORRO radar operating at 56 MHz and the EISCAT radars at VHF 224 and UHF 930 MHz. MORRO is deployed at the EISCAT installation near Tromsø in northern Norway home of the two other large incoherent scatter radars and the RF heating facility. It is known that under appropriate cycling of RF modification PMSE at the EISCAT VHF radar frequency shows an overshoot effect that is a result of the control of PMSE by charged dust particles. At the lower frequency of MORRO a different characteristic overshoot has been predicted by Chen and Scales (2005). In July 2008 a three-radar campaign was conducted involving MORRO the EISCAT VHF and UHF radars and the RF heater. Only weak effects of the heater on the PMSE measured by the 224 MHz radar were observed and a nearly absence of any effects on the PMSE measured by the 56 MHz radar, while the UHF radar showed intermittent enhancements of auroral particle precipitation. At one point PMSE enhancements were also detected by the UHF radar over three brief consecutive periods highly correlated with particle precipitation enhancements, as shown in Figs. 21 and 22.

The absence of the overshoot effect is possibly due to absorption of the heater wave in the lower D-region which may have depleted the heater wave in the lower part of the D-region thus explaining the near absence of the expected heater effects on PMSE, that is, the overshoot effect with different characteristics for the MORRO and EISCAT VHF radars.

C. La Hoz, O. Havnes, and M. Kassa Bekele, "Recent investigations of polar mesospheric summer echoes subject to RF modification with the MORRO and the EISCAT radars", Poster, AGU, 2009.

Differential scattering cross section of dusty plasma occurring PMSE

Based on the Born approximation in a dusty plasma, the differential scattering cross section of dusty plasma in the summer polar mesopause oc-

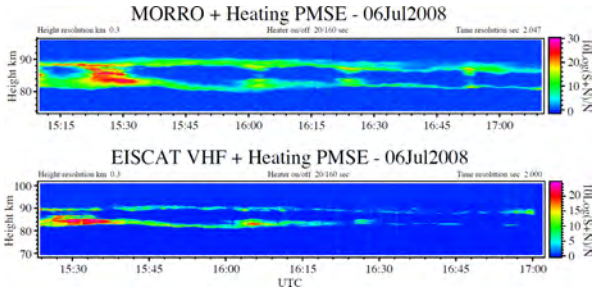

Figure 21: MORRO and EISCAT VHF data.

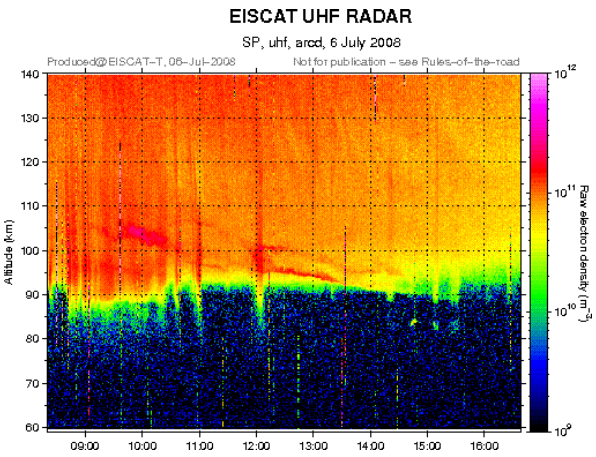

Figure 22: EISCAT UHF data.

curring PMSE is obtained as

$$\sigma_{\mathrm{d}}(\hat{o},\hat{i}) = \frac{3\pi^2\sigma_0\bar{n}_{\mathrm{e}}^2\sin^2\chi}{\left(\bar{n}_{\mathrm{i}}+\bar{n}_{\mathrm{e}}\right)^2}\frac{Z_{\mathrm{g}}^2N_{\mathrm{g}}}{\left(1+\mathbf{k}_{\mathrm{s}}^2\lambda_{\mathrm{D}}^2\right)^2}, \qquad (1)$$

where Z_{g} means grain charge, $\bar{n}_{\mathrm{i}}$ and $\bar{n}_{\mathrm{e}}$ the number density of ions and electrons respectively, λ_{D} the Debye length, σ_0 the Thomson scattering cross section, and χ the angle between the polarization of the incident wave and the direction of observation.

H. L. Li, et al., "Study on reflectivity and wavenumber occurring polar mesosphere summer echoes", Journal of Electromagnetic Waves and Applications 22(5—6), 803–814, 2008.

The layered dusty plasma structures in the polar summer mesopause

With reasonable assumptions, the traditional hydrodynamic equation is adopted to build a simplified theoretical model and the numerical method is used to simulate the formation and the evolution about these layered structures. The results indicate that the dynamical influence caused by

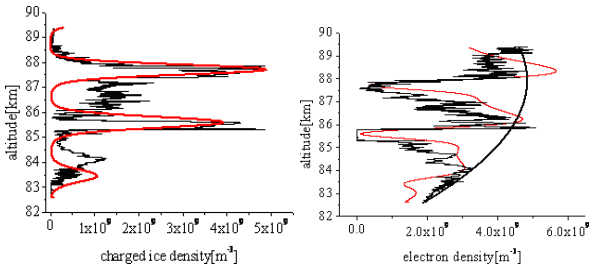

Figure 23: Left: Charged ice number density profile from the ECT02 rocket sounding (thin black line) and the model calculations (red line) with wavelength of 2.5 km and period of 4 hours. Right: Electron density profile from the ECT02 rocket sounding (thin black line) and the model results (red line).

gravity waves is an important factor in controlling the vertical transport of the heavy ice particles, making a significant contribution to convergence into these layered structures. To some extent, the multi-layered structures and the thickness of the layers depend on the ratio of the whole thickness of the ice particle layer to the vertical wavelength of the gravity waves. Furthermore, considering that gravity waves can also effectively modulate the ion density distribution, the ion motion under the influence of gravity waves has also been investigated, as well as simulating the electron density distribution according to the charge conservation laws. Finally, the simulation results are verified with the ECT02 rocket sounding data and shown by Fig. 23.

H. Li, et al., "Study on formation of the layered dusty plasma structures in the polar summer mesopause", Journal of Geophysical Research, SUBMITTED, 2009.

Mesosphere summer echoes observed by digital ionosonde

The data from DSP-4 at Zhongshan Station are analysed to study the irregular characteristics of the E and Es layers.

The results show that PMSE-like or PMSE-Es phenomena can be detected at MF and HF radar frequencies at Zhongshan Station and that the occurrence rate variations of PMSE-Es exhibit similarity to those of PMSE at multi-scales, such as seasonal, diurnal, and semidiurnal variation.

Meanwhile, based on the observed phenomena and experimental results in the Arctic, one can identify PMSE-Es according to two criteria proposed as below.

1. The virtual height of Es layer is not more than 90 km.
2. The virtual height of Es layer is not more than that of normal E layer.

H. L. Li, et al., "The statistics analysis of mesosphere summer echoes observed by DPS-4 at Zhongshan Station, Antarctica", Chinese Journal of Polar Research 19(1), 1—9, 2007.

Studies of macroscopic particles

Observations of the Iridium-Cosmos satellite collision debris

The EISCAT Scientific Association and the Inverse Problems and Modeling of Measurements group from the Sodankylä Geophysical Observatory have performed several beam-park measurements with the UHF and ESR radars after the Iridium-Cosmos satellite collision that occurred on February 10th 2009. This was a significant event, as it was the first time in the history of mankind that two satellites collided in space.

Beam-park measurements, such as the ones produced at EISCAT are useful, as they yield information about the shape and density of the ring-like debris cloud produced by the hyper-velocity collision. Measurements such as these are used e.g., to estimate collision probability between space debris and spacecraft. Fig. 24 shows debris detected using the EISCAT UHF system on May 14–15th 2009. The Iridium cloud orbital plane passes are visible at about 00:00 and 13:00 UT; and the Cosmos cloud pass at about 00:00 and 06:00 UT. The figure also compares the measurement with a statistical debris model called PROOF [Krag et al., Acta Astronautica, 2000], which is shown on the right-hand side. There are clear differences between the model and the measurement, which implies that the current debris model can be improved using the EISCAT measurements.

Space debris itself is an increasingly important environmental problem, as the amount of debris has been steadily growing in the last 60 years. Currently, it is estimated that there are about 600,000 objects larger than 1 cm in space today. Each of these objects are travelling at speeds of many kilometers per second, making them extremely hazardous for operational spacecraft. Some models even predict that the debris population is already in a collisional chain-reaction, the so called Kessler-syndrome, which will eventually render certain orbit regions unusable.

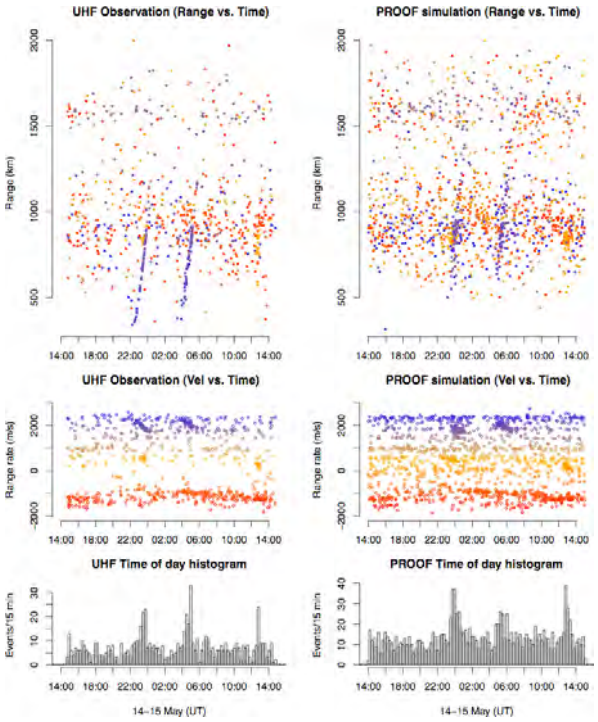

Figure 24: Measurement of space debris by the EISCAT UHF system on 14-15 May 2009 (left) and PROOF simulation (right).

J. Vierinen, et al., "Measuring space debris with phase coded aperiodic transmission sequences", Proceedings of the 5th European Conference on Space Debris, 2009.

J. Vierinen, J. Markkanen, and H. Krag, "High power large aperture radar observations of the Iridium-Cosmos collision", Proceedings of the 10th Advanced Maui Optical and Space Surveillance Technologies Conference, 2009.

Observations of meteor head echoes

Two examples of pulsating meteor events observed with the tristatic 930 MHz EISCAT UHF radar system were studied in detail. One of them provides the first strong observational evidence of a submillimeter-sized meteoroid breaking apart into two distinct fragments. The received power fluctuates regularly in the time profiles of all three receivers, but the fluctuation frequencies are different. The pulsations are interpreted as being due to interference from two distinct scattering centers and the three detected pulsation rates are utilized to calculate the differential velocity of the fragments. The result is consistent with interference from two fragments of unequal cross-sectional area over mass ratio, separating from each other

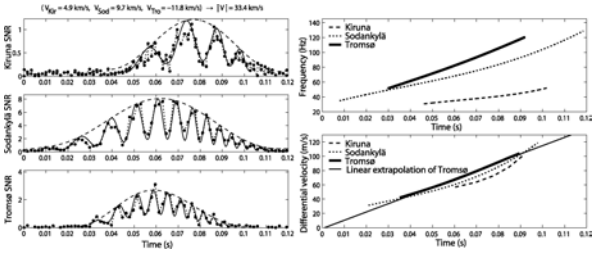

Figure 25: (left) The power profiles for a meteor detection with beat patterns of different frequencies. The dashed lines show the antenna beam patterns traced out along the meteoroid trajectory, the dots are the measured SNR, and the solid lines are modeled interference patterns. (right, top) The frequencies of the interference patterns versus time and (bottom) the corresponding differential velocity of two fragments separating along the RCS centroid trajectory.

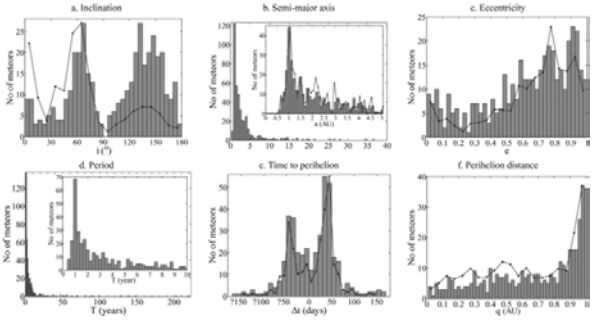

Figure 26: Histograms of orbital elements: (a) inclination, (b) semimajor axis, (c) eccentricity, (d) period, (e) time to perihelion and (f) perihelion distance. The semimajor axis and the period are also zoomed in to better illustrate the core of the distributions. Plotted in panels (a), (c) and (f) are also the inclination, eccentricity and perihelion distance distributions weighted with $v_\infty^{-3.1}$.

due to different deceleration along the trajectory of their parent meteoroid. The other meteor event is an example of a meteoroid undergoing quasi-continuous disintegration. This manifests itself as simultaneous pulsations at all three receivers. Both observations indicate a head echo target upper size limit of the order of half the 32 cm radar wavelength. See Fig. 25

J. Kero, et al., "Three-dimensional radar observation of a submillimeter meteoroid fragmentation", Geophysical Research Letter 35, L04101, doi:10.1029/2007GL032733, 2008.

Orbital characteristics of the tristatic EISCAT UHF meteors

The tristatic EISCAT 930-MHz UHF system is used to determine the absolute geocentric velocities of meteors detected with all three receivers simultaneously at 96 km, the height of the common radar volume. The data used in this study were taken between 2002 and 2005, during four 24-h runs at summer/winter solstice and vernal/autumnal equinox to observe the largest seasonal difference. The observed velocities of 410 tristatic meteors are integrated back through the Earth atmosphere to find their atmospheric entry velocities using an ablation model. Orbit calculations are performed by taking zenith attraction, Earth rotation as well as obliquity of the ecliptic into account. The results are presented in the form of different orbital characteristics. None of the observed meteors appears to be of extrasolar or asteroidal origin; comets, particularly short-period (< 200 yr) ones, may be the dominant source for the particles observed. About 40% of the radiants can be associated with the north apex sporadic meteor source and 58% of the orbits are retrograde. There is evidence of resonance gaps at semimajor axis values corresponding to commensurabilities with Jupiter, which may be the first convincing evidence of Jupiter's gravitational influence on the population of small sporadic meteoroids surveyed by radar. The geocentric velocity distribution is bimodal with a prograde population centred around 38 km/s and a retrograde population peaking at 59 km/s. The EISCAT radar system is located close to the Arctic Circle, which means that the North Ecliptic Pole (NEP) is near zenith once every 24 h, i.e. during each observational period. In this particular geometry, the local horizon coincides with the ecliptic plane. The meteoroid influx should therefore be directly comparable throughout the year. See Figs. 26 and 27.

C. Szasz, et al., "Orbit characteristics of the tristatic EISCAT UHF meteors", Monthly Notices of Royal Astronomical Society 388(1), 15–25, 2008.

Studies using ionospheric heating facilities

Excitation of artificial field-aligned irregularities

One of the most important phenomena discovered from ionospheric modification experiments is the excitation of artificial field–aligned irregu-

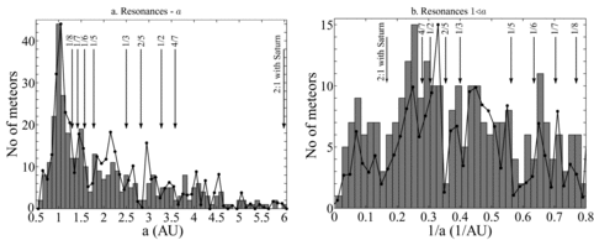

Figure 27: The distribution of (a) semimajor axis and (b) reciprocal semimajor axis. There are tendencies of resonance gaps at the values corresponding to commensurabilities with Jupiter and Saturn (arrows), most prominent in the weighted distributions.

larities (AFAIs). Their spatial scale is of the order of a few meters across and several kilometers along the magnetic filed line and their growth time is few seconds. Properties of striations appears to be understandable within the theory of thermal parametric (resonance) instability. A part of ionospheric modification experiments at high latitudes, utilizing the EISCAT HF heating facility at Tromsø, Norway (69.6°N, 19.2°E, $L = 6.2$, magnetic dip angle $I = 78°$), was concerned with studies of artificial field-aligned small-scale irregularities. Nonetheless there are a number of unclear issues related to the possibility of AFAI generation and seeking mechanisms of their formation when the ionosphere is heated by short pulses.

In the course of a Tromsø heating experiment on 27 October 2006 we have found evidence of AFAI excitation due to the pulsed HF pumping into the ionospheric F–region. The experiment was conducted in the day hours during quiet magnetic conditions. The HF facility was operated at 4912.8 kHz, O-mode of polarization. The phased array 2 was used. The HF antenna beam was varied by 6° steps allowing the direction of the HF beam at 3, 9 and 15° south from vertical pointing. The effective radiated power amounted to $P_{\text{eff}} = 210$ MW. The duration of heater-on cycles was varied between 3 and 7 min with a 3 min heater-off period. During each heater-on cycle pulses of duration $\tau = 384$ ms were radiated. Their repetition period was of $t = 4$ s.

AFAIs act as an artificially produced target for the diagnostic HF and VHF radio waves. Because of that the HF and VHF radars as well as bi-static scatter observations are widely used for studies of AFAIs. In the course of the experiment on 27 October, bistatic HF Doppler radio scatter observations were carried out on the London–Tromsø–St. Petersburg path at an operational frequency of

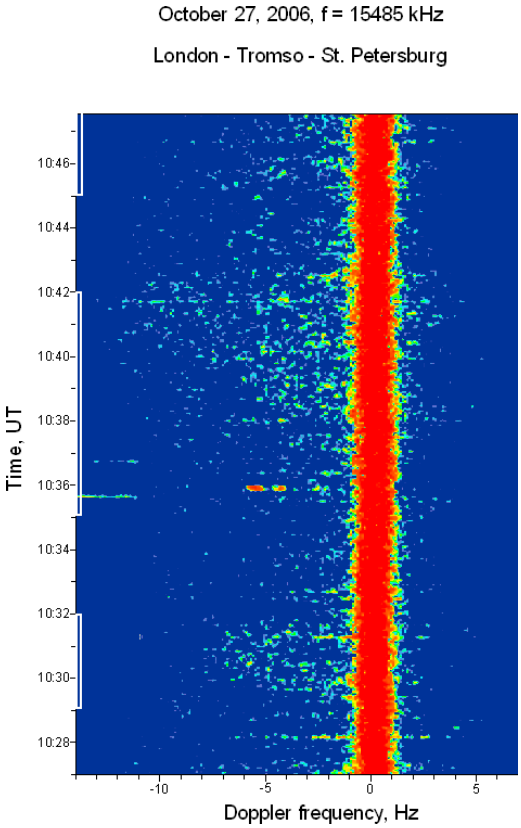

Figure 28: Dynamic Doppler spectra of HF diagnostic signals at 15,485 kHz on the London–Tromsø–St. Petersburg path on 27 October 2006 from 10:27 to 10:48 UT. During heater-on cycles from 10:29-10:32, 10:35–10:42, and 10.45–10.48 UT the HF antenna beam was tilted by 3, 9, and 15° to the south from vertical pointing correspondingly.

15,485 kHz. The diagnostic transmitter is located near London (52°N, 0°E) at a great circle distance of ∼2200 km from Tromsø. The reception of the diagnostic waves, scattered from field-aligned irregularities above Tromsø was made with a Doppler spectral method in St. Petersburg (60°N, 30.5°E) at a distance of ∼1200 km; the receiving antenna was directed towards Tromsø.

Figure 28 shows dynamic Doppler spectra of HF diagnostic signals at 15,485 kHz on the London–Tromsø–St. Petersburg path on 27 October 2006.

As can be seen from Fig. 28, the intensity and width of Doppler spectra of scattered signals strongly depends on HF aspect angle. The most intense scattered signals were observed from 10:35–10:42 UT, when the direction of HF beam was close to the field-aligned pointing. Figure 29

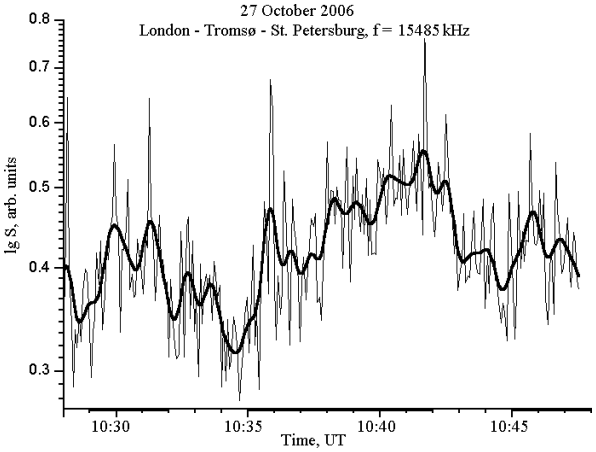

Figure 29: Variations in spectral power of HF diagnostic signals at 15,485 kHz on the London–Tromsø–St. Petersburg path on 27 October 2006 from 10:27 to 10:48 UT.

shows variations in spectral power for the same event.

It is interesting to note that the intensity of scattered signals rises during the heater-on cycle from 10:35–-10:42 UT, reaching maximum to the end of cycle. When the heating facility was turned off the decay time of scattered signals continued up to the beginning of the next heater-on period.

What is the mechanism of AFAI excitation when HF pumping is produced by short pulses? The average radiated power $P_{\rm av}$ with allowance for the pulse duty cycle $Q = t/\tau$ can be estimated as $P_{\rm av} = P_{\rm eff}/Q$. Thus during the heating experiment on 27 October the average radiated power was about of $P_{\rm av} = 0.34$ MW. Keeping in mind that the threshold powers for AFAI generation cutoff are of the order of $P_{\rm thr} = 0.3$—0.5 MW, the average radiated power was comparable with $P_{\rm thr}$. Along with that, it is reasonable to assume that under considered conditions the AFAIs can be generated due to parametric decay instability development. This question needs further clarification. The results obtained give evidence for a pronounced magnetic zenith effect in the AFAI behavior.

N. F. Blagoveshchenskaya, et al., "Phenomena initiated by ionospherere modification caused by powerful HF radio waves at different latitudes", Solar-Terrestrial Physics 12(2), 206—209, 2008.

N. F. Blagoveshchenskaya, et al., "The polar-ionosphere phenomena induced by high-power radio waves from the SPEAR heating facility", Radiophysics and Quantum Electronics 51(11), 847—857, 2008.

Diagnostic radio wave heating in the mesosphere using cross-modulation

In June–July 2008, the HF facility (Heater) and Dynasonde were used together to measure the effect of radio wave heating on the plasma in the D-layer ionosphere. The Dynasonde measured the change in absorption of a 2 MHz wave reflected from the E-region. On alternating Dynasonde probing pulses, the D-region was subject to radio wave heating in a form of the classic "cross-modulation" experiment. The heater modification wave was set to a high enough frequency (e.g. 5.4 MHz) to prevent reflection. The VHF radar was used to estimate the D-region electron density. The diagnostic wave absorption is a function of electron density, which remains constant, and the temperature-dependent electron collision frequency. Hence, by comparing the absorption of the diagnostic wave for heater on and off intervals, and varying the phasing between the diagnostic and pump pulses, a height-resolved estimate of the pump-enhanced electron temperature in the D-layer can be generated. Figure 30 shows the data from the cross-modulation experiment run on 2 July 2008. The top panel shows electron densities from VHF radar. The middle panel shows the change in 2 MHz absorption (from unheated to heated ionosphere) with altitude. The bottom panel shows the power of 2 MHz E-region echo. A preliminary analysis of the results suggests that conventional D-region radio heating models greatly overestimate the change in absorption, possibly by an order of magnitude. If this translates into an error in the estimated heating, this could be important for the use of radio heating in remote sensing of PMSE, PMWE and other ionospheric phenomena.

A. Senior, M. T. Rietveld, and M. J. Kosch, "Radio wave heating of the plasma in the polar mesosphere diagnosing using crossmodulation", EISCAT Workshop, 2009.

Parametric modification by ionospheric heating

The non-Maxwellian factor due to ionosphere heating must be considered in the inversion of incoherent scatter power spectra. Using the super-Gaussian electron distribution function,

$$f_{\rm e}(v) = \frac{m}{4\pi v_{T_{\rm e}}^3 \Gamma\left(3/m\right)} \exp\left[-\left(v/v_{T_{\rm e}}\right)^m\right], \quad (2)$$

the incoherent scatter spectrum recorded with UHF system at UT 10:22 on 15 Aug. 2006 in an EISCAT heating campaign conducted by China, was

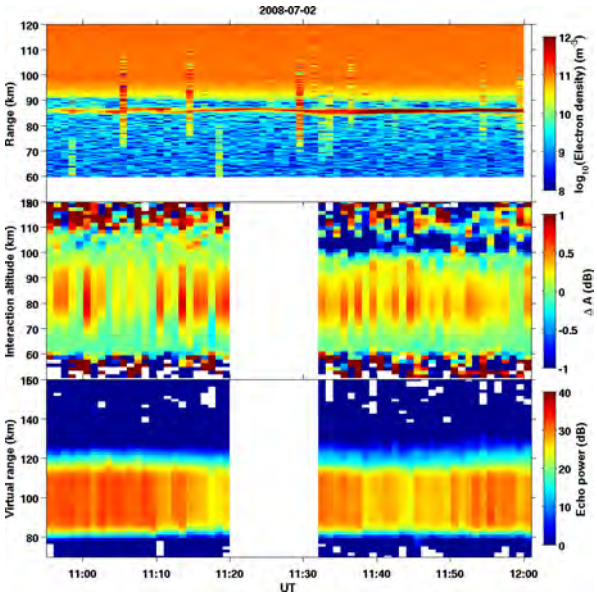

Figure 30: Top panel: electron densities from VHF radar. Middle panel: change in 2 MHz absorption (from unheated to heated) with altitude. Bottom panel: power of 2 MHz E-region echo.

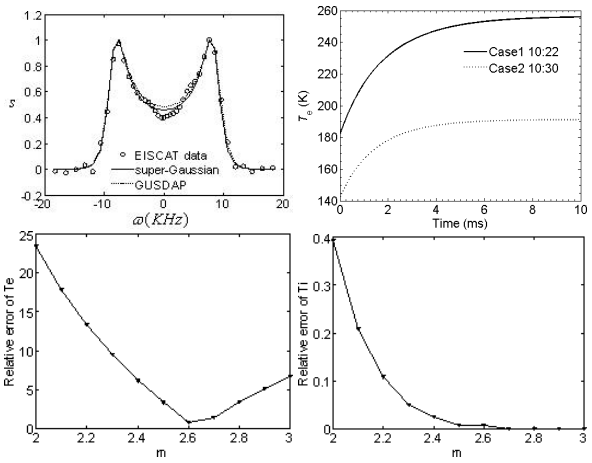

Figure 31: Top left: IS spectrum due to ionospheric heating at UT 10:22 15 Aug. 2006 in Tromsø. Top right: IS spectrum due to ionospheric heating at UT 10:22 15 Aug. 2006 in Tromsø. Bottom left: Relative error of T_e with m. Bottom right: Relative error of T_i with m.

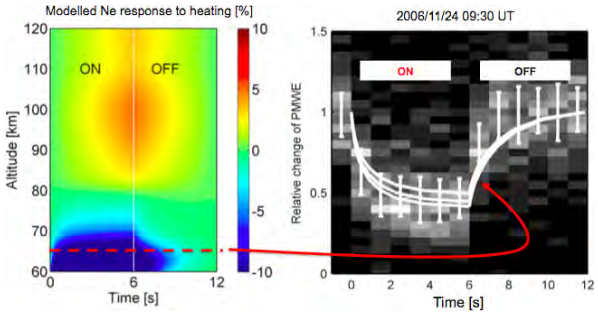

Figure 32: Modelled N_e response to heating.

inversed as indicated by top left panel of Fig. 31. The figure shows that at an altitude of 186.72 km, the result is consistent with IS spectrum obtained through GUSDAP and raw data. Also, in the top right panel of Fig. 31, we see that the 37% and 46% enhancements of electron temperature at the universal time of 10:22 and 10:30 respectively.

In addition, the effect of a non-Maxwellian index m on the plasma temperature was studied. The bottom left panel of Fig. 31 shows that the extended tail of electron distribution function can cause that electron temperature is overestimated and its relative error is up to 25%. We also see that the ion temperature has the opposite effect, as indicated by the bottom right panel of Fig. 31.

B. Xu, et al., "Temperature enhancement induced by ionosphere heating in low altitude region", Progress in Natural Science 18(11), 1339—1343, 2008.

B. Xu, et al., "Incoherent scatter spectra from plasma of a 13-moment approximation distribution function", Science in China Series E: Technological Sciences 51(5), 624—631, 2008.

Polar mesosphere winter echo (PMWE) modulation in active HF heating experiments

In this study, we propose for the first time a possible mechanism for the Polar Mesosphere Winter Echo (PMWE) modulation in the active HF heating experiments. The mechanism is based on the increased negative ion production due to heating. This study opened new perspectives for observing the mesospheric composition and it will potentially lead to several important papers within the next few years. See Fig. 32.

A. Kero, et al., "Could negative ion production explain the polar mesosphere winter echo (PMWE) modulation in active HF heating experiments?", Geophysical Research Letters 35(23), L23102, doi:10.1029/2008GL035798, 2008.

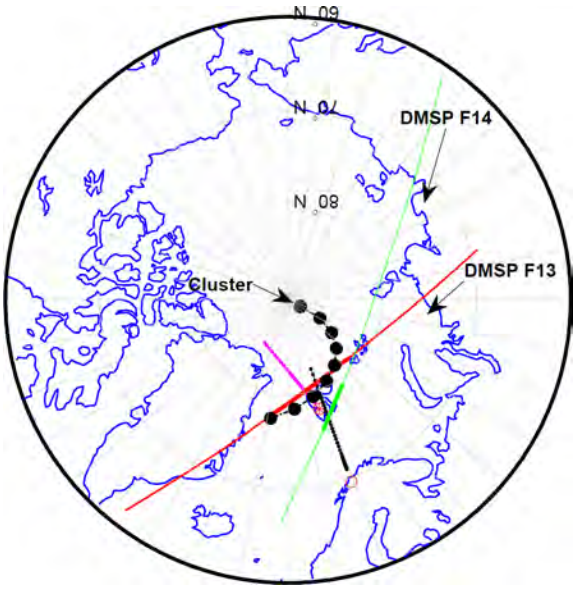

Figure 33: Geometric configuration of Cluster, DMSP and the EISCAT radars on 12 February 2003. The footprint of the Cluster SC1, predicted by the T96 model between 08:00 and 12:00 UT, is plotted at 30-min time intervals as a black dot. Overpasses of DMSP F13 and F14, as well as radar beams are also displayed in the figure. Black arrows indicate the direction of travel of the spacecraft.

Combined EISCAT and satellite studies

The Cluster–EISCAT campaign

On 12 February 2003, the EISCAT/ESR radar was operating in support of the Cluster mission for a cusp study. During the interval, from 08:00 to 12:00 UT, the IMF B_z component underwent four reversals, remaining for around 30 min in each orientation. Here we present a comparative study of the cusp, based on observations from spaceborne and ground-based instrumentation. The geometric configuration of the EISCAT, Cluster and DMSP are shown in Fig. 33.

During the interval, both Cluster and the EISCAT were, on occasion, observing the cusp region. The series of IMF reversals resulted in a sequence of poleward and equatorward motions of the cusp; consequently Cluster crossed the high-altitude cusp twice before finally exiting the dayside magnetopause, both times under conditions of northward IMF B_z. The first magnetospheric cusp encounter, by all four Cluster spacecraft, showed reverse ion dispersion typical of lobe reconnection; subsequently, Cluster spacecraft 1 and 3 (only) crossed the cusp for a second time. We suggest that, during this second cusp crossing, these two spacecraft were likely to have been on newly closed field lines, which were first reconnected (opened) at low latitudes and later reconnected again (re-closed) poleward of the northern cusp. See Fig.34.

At ionospheric altitudes, the latitudinal excursions of the cusp/cleft region in response to the series of the IMF polarity changes were clearly captured by both the ESR and the þykkvybær radar of the SuperDARN HF network. The Open-Closed field-line Boundary (OCB) inferred from the HF radar observations underwent latitudinal variations in response to the IMF polarity changes that are in accordance with those predicted by Newell et al. (1989). Furthermore, variations in the ionospheric parameters yielded by the EISCAT VHF and ESR radars are basically consistent with inferences drawn from the HF radar observations. We conclude that Cluster spacecraft 1 and 3 crossed the cusp for a second time as a result of the latitudinal migration of the cusp in response to the IMF polarity reversals; at that time, however, the cusp lay poleward of spacecraft 4. Snapshots of the cusp from two DMSP satellite passes provide further support for this interpretation.

H. T. Cai, et al., "Observations of the cusp during successively stable northward/southward turning IMF", Geophysical Research Abstracts, V10, EGU2008-A-08506, EGU General Assembly, 2008.

H. T. Cai, et al., "Cusp observations during a sequence of fast IMF B_z reversals", Annales Geophysicae 27(7), 2721-–2737, 2009.

Observations of ion dispersion and electron density fluctuations with the REIMEI satellite and the EISCAT Svalbard Radar

This research employs results from co-ordinated measurements between the Japanese low altitude REIMEI satellite and the EISCAT Svalbard Radar—shown in Figs.35 and 36 respectively—and other ground-based instruments. The results are related to the dayside cusp where clear signatures of ion dispersion were observed by the satellite particle instrument in the form of three distinct steps in the ion energy and possibly two more as shown in Fig. 36. Fast variations of electron flux and energy took place during the events of ion dispersion. It has been demonstrated that the

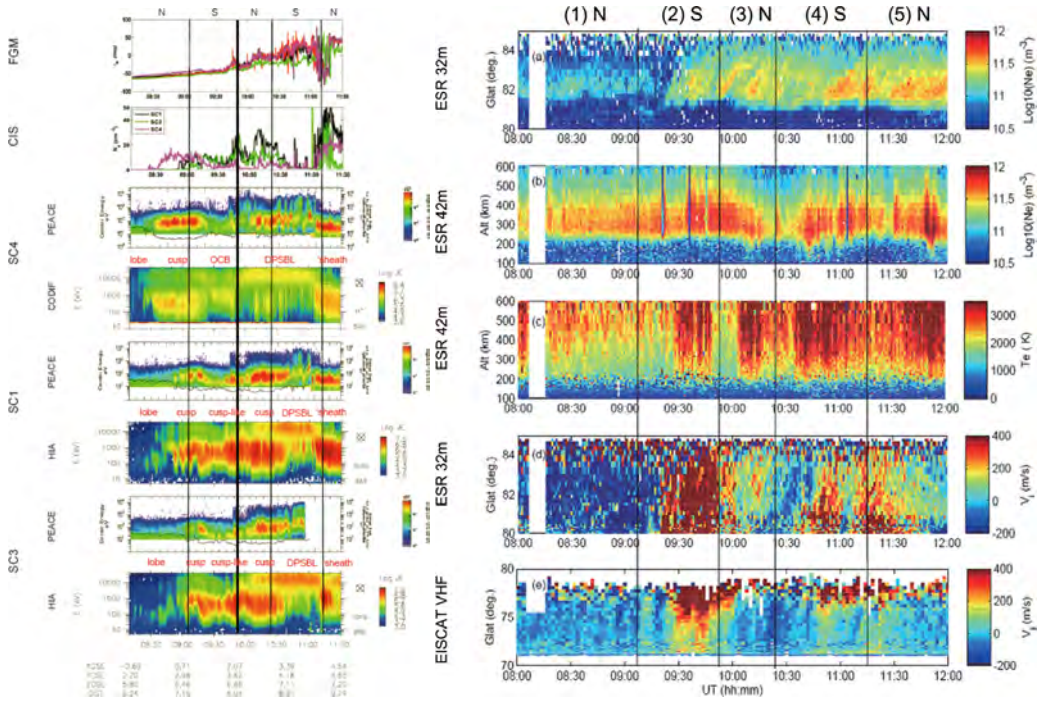

Figure 34: Observations from Cluster (left column) and the EISCAT facilities (right column).

majority of the observed cusp structured ion dispersion events are most likely related to magnetopause reconnection produced in an intermittent manner by temporal cusp features rather than by a stationary one. The small scale (<5 km) and fast electron fluctuations (<1 s) were found to be most probably due to reconnection processes. Magnetic reconnection is the primary form of coupling between the solar wind and the Earth's magnetosphere by which the bulk of solar wind energy is transferred to the magnetosphere and subsequently to the ionosphere.

J. Lunde, et al., "Ion-dispersion and rapid electron fluctuations in the cusp: A case study", Annales Geophysicae 26(8), 2485—2502, 2008.

The CHAMP - EISCAT campaign

The combined CHAMP-EISCAT campaign was scheduled to run in October 2006 in order to observe characteristic features of the ionosphere and thermosphere in the cusp region simultaneously. The thermospheric components, namely the mass density and the density anomaly revealed typical cusp features. CHAMP crosses the radar stations at least once per operation time in less than 11° longitudinal distance providing neutral air mass density values.

Figure 37 shows the ionospheric parameters obtained with the field-aligned ESR 42 m antenna (left) and the Tromsø VHF radar which was pointing northward with an elevation angle of 30°. The overpasses of CHAMP are marked with vertical lines. At these overpasses CHAMP observed the thermospheric total mass density using the accelerometer readings taken onboard the spacecraft. The total mass density and the thereof derived density anomalies for the three orbits are shown in Fig. 38. During the earliest overflight both quantities do not reveal any significant enhancement at the cusp latitudes and in the second overflight they differ only marginally from the other parts. During the third overflight, however, an enhancement in the density and density anomaly is identified.

The ionospheric parameters derived from the EISCAT radar measurements, were used together with density of neutral gas species (derived from MSIS) and geomagnetic parameters to estimate height-integrated Hall and Pedersen conductivities for the periods of interest which are presented in Fig. 39. Taking these parameters into account the Joule heating rates for the overpasses of CHAMP were estimated considering both, large-scale and small-scale, components of the effective electric field. Consequently, the estimated heating rates are larger (by a factor of 5) than those ob-

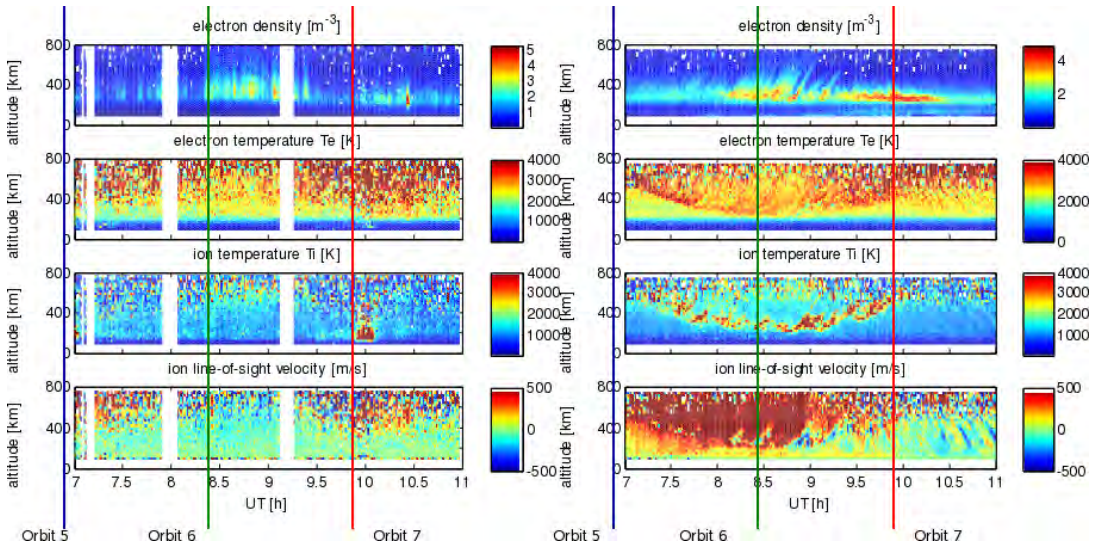

Figure 37: Ionospheric parameters (electron density, electron temperature, ion temperature and ion line-of-sight velocity on October 13th, 2006, observed by the ESR 42 m antenna (left) and the Tromsø VHF radar (right). The enhanced electron density is regarded as a cusp feature. Two overpasses of CHAMP took part during the observation hours.

tained in previous campaigns. The heating rates are largest during the CHAMP overpass which was assumed to be closest to the cusp. Two components might be responsible for the increased Joule heating: a heated layer above the E region and an increased electric field strength. The uplift of the heated layer is due to the impact of soft particle precipitation in the cusp. Changes in the amount of energy per volume deposited in this layer correspond well to the mass density variations as observed with CHAMP. The merging electric field is considered to provide the power needed for the heating. The density anomaly is then a consequence of local composition changes due to differential expansion.

S. Rentz, "The upper atmospheric fountain effect in the polar cusp region", PhD thesis, Technische Universität Carolo-Wilhelmina zu Braunschweig, 2009.

High-latitude effects of a fast solar wind stream

UHF and VHF radar observations were made during 8–9 March 2008 of the ionospheric effects of a fast solar wind stream from a low-latitude coronal hole which traversed the sub-Earth helio-meridian in early March 2008. The timing of the observations was predicted by extrapolation of previous crossings of the coronal hole. The prediction was sufficiently accurate to ensure that observations included both the start and the peak of the ionospheric activity. The VHF radar data for the period 1200 UT on March 8th to 0900 UT on March 9th is shown in Fig. 40. Ongoing analysis involves comparing the spectrum derived from the EISCAT data with the energetic electron spectrum from the five Themis spacecraft.

Theoretical studies

On the incoherent scatter spectra

Considering the non-Maxwellian high-tail of electron distribution function induced by HF heating, the incoherent scatter spectra of collisional plasma with the Lorentzian distribution were investigated. The ion line spectra with $\kappa = 3$, 5 and ∞ (Maxwellian), given by the top left panel of Fig. 41, show that with the decrease in κ, the peak-to-valley ratio, $R_{\rm pv}$, augments and peak power, $P_{\rm max}$, declines. Also, as shown by the top right panel of Fig. 41, with an increase of collision frequency, the spectrum becomes narrower and the peak power declines. Furthermore, the effects of non-Maxwellian index, κ, on the ion resonance frequency, $\omega_{\rm irf}$, and half-power spectrum width are not as obvious as that of collisional frequency, but both the non-Maxwellian index and the collisional frequency have an important influence on the peak power of the ion line spectra and the inverse function on the peak-to-valley ratio.

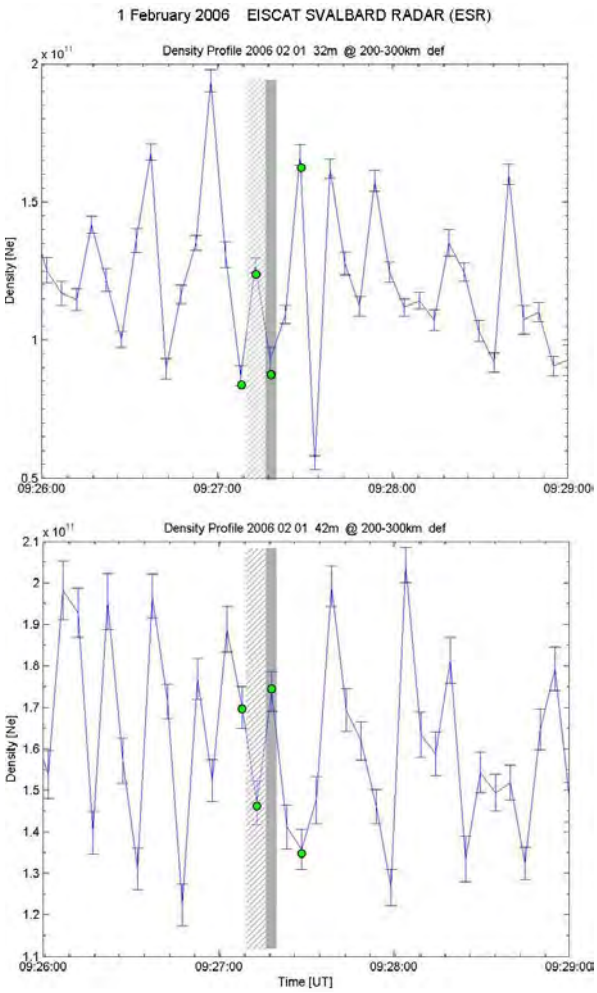

Figure 35: Plot of the raw electron density versus time measured with the 32 m antenna (upper figure) and the 42 m antenna (lower figure). The integration in height is 100 km. Note the anti-correlation between the 32 m and 42 m during the time of interest, marked with green circles at ∼09:27:08 UT, ∼09:27:13 UT, ∼09:27:19 UT and ∼09:27:28 UT. The diagonally shaded area corresponds to data dumps taken when the REIMEI passes over the 32 m antenna beam, while the shaded area indicates the start of the main ion step in the energy dispersion.

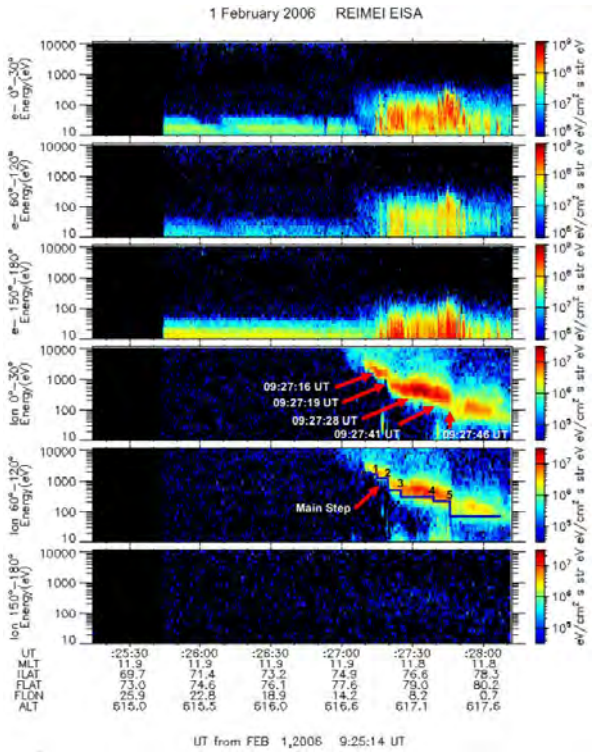

Figure 36: In this REIMEI EISA plot, the 3 upper panels show the electron flux and energy versus time. The first from top is for pitch angles 0°-30° (down), the second for 60°–120° and the last for 150°–180° (up). The 3 lower panels display ion flux and energy correspondingly. The stepped ion-energy-dispersion is marked with red arrows and their respective start time. The largest transition is the second step, which are marked as the main step.

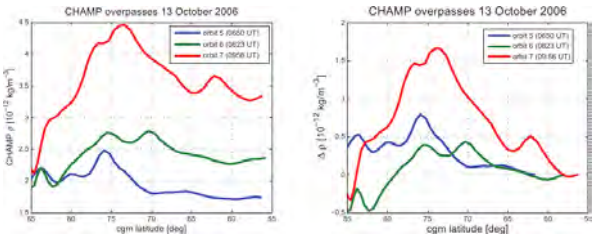

Figure 38: CHAMP-observed density (left) and density anomaly $\Delta\rho$ (right) along three passes over the EISCAT facilities on October 13th, 2006. The enhancement in the vicinity of the cusp is most prominent during the latest overpass.

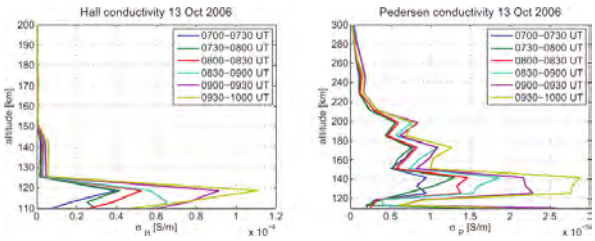

Figure 39: Altitude profiles of Hall conductivity (left) and Pedersen conductivity (right) for different times of the observation period on October 13th, 2006.

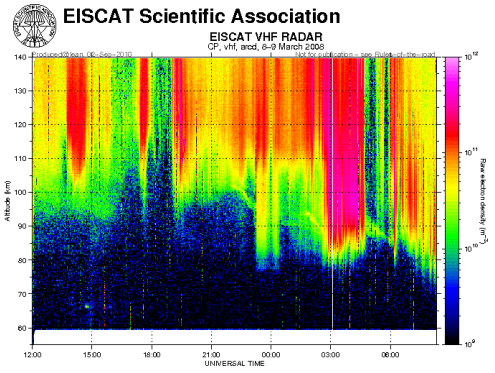

Figure 40: VHF radar data from 8-9 March 2008, covering the fast solar wind stream from a low-latitude coronal hole.

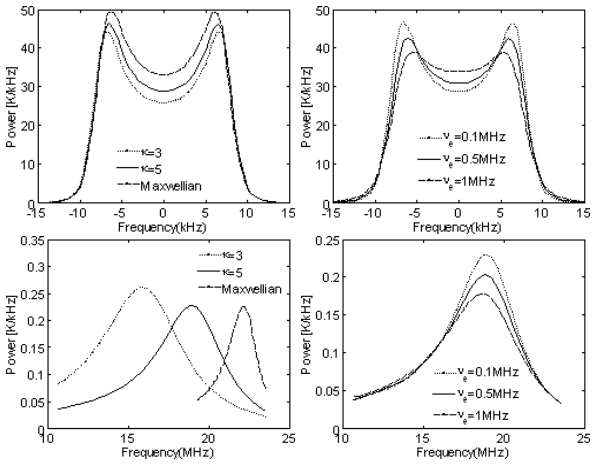

Figure 41: Top left: The variation of ion line with non-Maxwellian index. Top right: The variation of ion line with collisional frequency. Bottom left: The variation of plasma line with non-Maxwellian index. Bottom right: The variation of plasma line with collisional frequency.

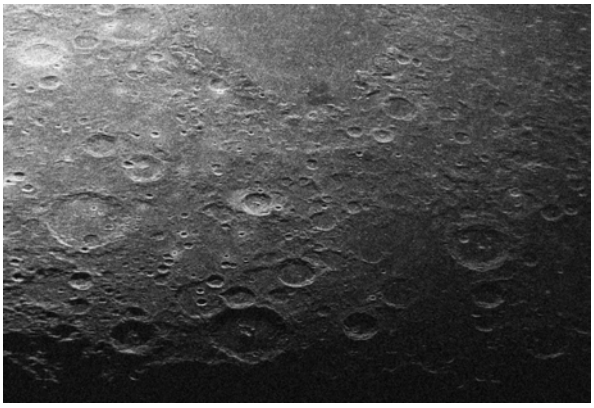

Figure 42: Lunar map by the EISCAT UHF radar.

In addition, as indicated by the lower panels of Fig. 41, with the increase in non-Maxwellian index, the amplitude and the width of plasma line increase, and the resonance frequency shifts. No effect from the collisional frequency is seen on the resonance frequency, but it plays a significant role in the peak power.

Z. S. Wu, et al., "Incoherent scatter spectra of collisional plasma with the Lorentzian distribution", at URSI General Assembly, Chicago, 2008.

New uses of EISCAT

Lunar radar mapping

During December 2008, the Inverse Problems and Modeling of Measurements group from Sodankylä successfully applied the EISCAT UHF radar for Lunar range-Doppler mapping purposes. One of the un-focused opposite circular polarized radar images produced during the campaign is shown in Fig. 42.

Polarimetric radar studies of the Moon are useful as they provide a way of probing the subsurface geochemical properties and the rock abundance of lunar regolith. Due to the lack of erosion, the Moon is thought to contain important clues on the formation of the Earth-Moon system and the statistics of meteoroidal and asteroidal impacts on Earth. Lunar regolith is also a viable source for the ^{3}He isotope, which is one possible fusion reactor fuel.

Previously, lunar radar maps have been produced at wavelengths of 3.8 cm, 70 cm, and 7.5 m. The 32-cm wavelength used by the EISCAT UHF system has not earlier been used for such studies. Different wavelengths probe the surface at different depths. Echo intensity also tells of the surface

roughness at the radar wavelength scales. A 32 cm map would provide valuable information to complement space probe measurements and other previously published high resolution Lunar maps.

There are still several challenges in terms of Doppler North-South ambiguity mitigation, focusing, and clock error mitigation. These issues will be addressed by developing improved analysis procedures and by performing new measurements with the EISCAT UHF radar.

J. Vierinen and M. S. Lehtinen, "32-cm wavelength radar mapping of the moon", Proceedings of the 6th European Radar Conference, 2009.

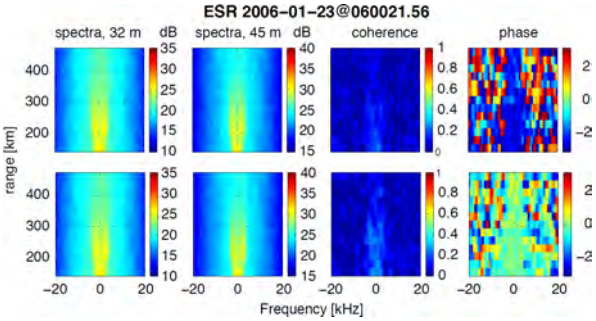

Figure 43: Spectral measurements of incoherent scatter from a quiet ionosphere made with the two ESR antennas in interferometric mode.

Radar interferometer phase calibration using the visibility function of incoherent scattering

Aperture synthesis imaging radar (ASIR) has become a powerful technique to make measurements of ionospheric dynamic structures in three dimensions (3-D). The technique works as expected provided the relative phases of the signals measured by the aperture receivers are due only to the different propagation paths of the signals from the source. This condition demands phase calibration to eliminate the changes in phase introduced by the equipment, which are normally uncontrollable. A novel procedure to calibrate the phases of an interferometric radar that is capable to detect the incoherent scatter signals from electrons in the Earth's ionosphere has been developed. Under conditions that are usually fulfilled in actual experiments it is shown that the visibility function of incoherent scattering radar signals arising from thermal fluctuations of electron density in the ionosphere is a real function. This implies that the phase of the visibility function is constant and equal to zero. This fact affords a practical procedure to make global relative calibration of the baseline phases of an aperture synthesis radar interferometer used for ionospheric imaging. An example of actual measurements and calibration made with the two antenna system of the EISCAT Svalbard Radar is shown in Fig. 43 which shows spectral measurements of incoherent scatter from a quiet ionosphere made with the two ESR antennas in interferometric mode. The first column shows height spectrograms measured by the 32 m antenna, which was also the transmitter antenna; while the second column contains the spectrograms measured by the 45 m antenna; the third and fourth columns show the amplitude and phase of the normalized visibility respectively. The first row shows the direct measurements, while the second row shows the amplitude and the phase of the normalized visibility function after the phase calibration has been carried out, which in this case was to set the phases of the signal amplitudes of the two receivers equal to zero (or, equivalently, to two arbitrary equal values, the result being the same). It can be seen that after the calibration has been performed, the coherence amplitude has improved a bit, being around 0.3 instead of 0.2 before the calibration. This is to be expected, since a non-zero phase difference between the two signals implies destructive interference to a more or less degree, depending on the value of the phase difference, upon mixing them. This work—funded partly by the research council of Norway—is a contribution to the EISCAT_3D Design Study funded by the EU's Framework Programme 6 (FP6).

T. Grydeland and C. La Hoz, "Phase calibration of a radar interferometer by means of incoherent scattering", Radio Science(45), RS4001, doi:10.1029/2009RS004249, 2010.

List of publications, 2008

Aikio, A. T., T. Pitkänen, D. Fontaine, I. Dandouras, O. Amm, A. Kozlovsky, A. Vaivdas, and A. Fazakerley, EISCAT and Cluster observations in the vicinity of the dynamical polar cap boundary, Ann. Geophys., 26, 87–105, 2008.

Alfonsi, L., A. J. Kavanagh, E. Amata, P. Cilliers, E. Correia, M. Freeman, K. Kauristie, R. Liu, J.-P. Luntama, C.N. Mitchell, G.A. Zherebtsov, Probing the high latitude ionosphere from ground-based observations: The state of current knowledge and capabilities during IPY (2007–2009), J. Atmos. Solar Terr. Phys., 70, 18, 2293-2308, doi:10.1016/j.jastp.2008.06.013, 2008.

Amm, O., A. Aruliah, S.C. Buchert, R. Fujii, J. W. Gjerloev, A. Ieda, T. Matsuo, C. Stolle, H. Vanhamäki, and A. Yoshikawa, Towards understanding the electrodynamics of the 3-dimensional high-latitude ionosphere: present and future, Ann. Geophys., 26, 3913–3932, 2008.

Balan, N., H. Alleyne, S. Walker, H. Reme, I. McCrea, A. Aylward, Magnetosphere-ionosphere coupling during the CME events of 07-12 November 2004, J. Atmos. Solar Terr. Phys., 70, 17, 2101–2111,doi:10.1016/j.jastp.2008.06.015, 2008.

Beharrell, M., and Honary, F., A new method for deducing the effective collision frequency profile in the D-region, J. Geophys. Res., 113, A05303, doi:10.1029/2007JA012650, 2008.

Belova, E., M. Smirnova, M.T. Rietveld, B. Isham, S. Kirkwood, and T. Sergienko, First observation of the overshoot effect for polar mesosphere winter echoes during radiowave electron temperature modulation, Geophys. Res. Lett., 35, L03110, doi:10.1029/2007GL032457, 2008.

Blagoveschenskaya, N.F, T.D. Borisova, V.A. Kornienko, T.R. Robinson, T.K. Yeoman, V.L. Frolov, M.T. Rietveld, Phenomena initiated by ionosphere modification caused by powerful HF radio waves at different latitudes, Solar-Terrestrial Physics (in Russian), 12, 2, 206–209, 2008.

Blagoveshchenskaya, N. F., T. D. Borisova, V. A. Kornienko, A. S. Janzhura, A. S. Kalishin, T. R. Robinson, T. K. Yeoman, D. M. Wright, and L. J. Baddeley, The polar-ionosphere phenomena induced by high-power radio waves from the spear heating facility, Radiophysics and Quantum Electronics, 51, 11, 847–857, doi:10.1007/s11141-009-9089-z, 2008.

Breen, A.R., R.A. Fallows, M.M. Bisi, R.A. Jones, B.V Jackson, M. Kojima, G.D. Dorrian, H.R. Middleton, P. Thomasson and G. Wannberg, "The solar eruption of 13 May 2005 and its effects: Long-baseline interplanetary scintillation observations of the Earth-directed coronal mass ejection", Astrophysical Journal Letters, 683, L79-L82, 2008.

Buchert, S.C., T. Tsuda, R. Fujii, and S. Nozawa, The Pedersen current carried by electrons: a non-linear response of the ionosphere to magnetospheric forcing, Ann. Geophys., 26, 2837–2844, 2008.

Carlson, H.C., K. Oksavik, and J. Moen, On a new process for cusp irregularity production, Ann. Geophys., 26, 2871–2885, 2008.

Dahlgren, H., N. Ivchenko, B.S. Lanchester, J. Sullivan, D. Whiter, G. Marklund, and A. Strømme, Using spectral characteristics to interpret auroral imaging in the 731.9 nm O+ line, Ann. Geophys., 26, 1905–1917, 2008.

Dorrian, G.D., A.R. Breen, D.S. Brown, J.A. Davies, R.A. Fallows, and A.P. Rouillard, Simultaneous interplanetary scintillation and Heliospheric Imager observations of a coronal mass ejection, Geophys. Res. Lett., 35, L24104, doi:10.1029/2008GL036181, 2008.

Enell, C.-F., P.T. Verronen, M.J. Beharrell, J.P. Vierinen, A. Kero, A. Seppälä, F. Honary, T. Ulich, and E. Turunen, Case study of the mesospheric and lower thermospheric effects of solar X-ray flares: coupled ion-neutral modelling and comparison with EISCAT and riometer measurements, Ann. Geophys., 26, 2311–2321, 2008.

Fallows, R.A., A.R. Breen, and G.D. Dorrian, Developments in the use of EISCAT for interplanetary scintillation, Ann. Geophys., 26, 2229–2236, 2008.

Friedrich, M., M. Fankhauser, A steady-state model for the D- to F -region of the polar cap, Adv. Space Res., 42, 4, 703–706, doi: 10.1016/j.asr.2007.06.077, 2008.

Griffin, E.M., A.L. Aruliah, I. McWhirter, H.-C. I. Yiu, A. Charalambous, and I. McCrea, Upper thermospheric neutral wind and temperature measurements from an extended spatial field, Ann. Geophys., 26, 2649–2655, 2008.

Grydeland, T., B. Gustavsson, L.J. Baddeley, J. Lunde, and E.M. Blixt, Conditional integration of Incoherent Scattering in relation to flickering aurora, J. Geophys. Res., 113, A08305, doi:10.1029/2008JA013039, 2008.

Gustavsson, B., M.J. Kosch, A. Senior, A. Kavanagh, U. Brandstrom, and E.M. Blixt, Combined EISCAT Radar and Optical Multi-Spectral and Tomographic Observations of Black Aurora, J. Geophys. Res., 113, A06308, doi:10.1029/2007JA012999, 2008.

Gustavsson, B., and B. Eliasson, HF radio wave acceleration of ionospheric electrons, Analysis of HF-induced optical enhancements, J. Geophys. Res., 113, A08319, doi:10.1029/2007JA012913853-866, 2008.

Häggström, Ingemar, Incoherent Scatter Radar Measurements of Field Aligned Currents in the Polar Region, Proceedings of Radio Science and Communications & Mathematical Modelling of Wave Phenomena (Eds. Sven Nordebo and Börje Nilsson), RVK08/MMWP08, ISSN 1650-2647, 145–147, 2008.

Kero, Antti, Ionospheric D-region studies by means of active heating experiments and modelling, PhD thesis, University of Oulu, Finland. ISBN 978-951-42-8915-6, 2008.

Kero, A., J. Vierinen, C.-F. Enell, I. Virtanen, and E. Turunen, New incoherent scatter diagnostic methods for the heated D-region ionosphere, Ann. Geophys., 26, 2273–2279, 2008.

Kero, A., C.-F. Enell, A. J. Kavanagh, J. Vierinen, I. Virtanen, and E. Turunen, Could negative ion production explain the polar mesosphere winter echo (PMWE) modulation in active HF heating experiments?, Geophys. Res. Lett., 35, L23102, doi:10.1029/2008GL035798, 2008.

Kero, Johan, High resolution meteor exploration with tristatic radar methods, PhD thesis, IRF Scientific Report 293, ISBN 978-91-977255-3-8, March 2008.

Kero, J., C. Szasz, G. Wannberg, A. Pellinen-Wannberg, and A. Westman, On the meteoric head echo radar cross section angular dependence, Geophys. Res. Lett., 35, L07101, doi:10.1029/2008GL033402, 2008.

Kero J., C. Szasz, A. Pellinen-Wannberg, G. Wannberg, A. Westman, and D. D. Meisel, Three-dimensional radar observation of a submillimeter meteoroid fragmentation, Geophys. Res. Lett., 35, L04101, doi:10.1029/2007GL032733, 2008.

Kero, J., C. Szasz, A. Pellinen-Wannberg, G. Wannberg, A. Westman, and D. D. Meisel, Determination of meteoroid physical properties from tristatic radar observations, Ann. Geophys., 26, 2217–2228, 2008.

La Hoz, C., and O. Havnes, Artificial modification of Polar Mesospheric Winter Echoes (PMWE) with an RF heater: Do charged dust particles play an active role?, J. Geophys. Res., 113, D19205, doi:10.1029/2008JD010460, 2008.

Lehtinen, M. S., I. I. Virtanen, and J. Vierinen, Fast comparison of IS radar code sequences for lag profile inversion, Ann. Geophys., 26, 2291–2301, 2008.

Lukianova, R., A. Kozlovsky, and T. Turunen, Comparison and validation studies related to the modeling ionospheric convection and the European incoherent scatter observations in the polar cap, Int. J. Geomagn. Aeron., 7, 3, GI3005, 10.1029/2007GI000169, 2008.

Lunde, J., S. C. Buchert, Y. Ogawa, M. Hirahara, K. Seki, Y. Ebihara, T. Sakanoi, K. Asamura, M. Okada, T. Raita, and I. Häggström, Ion-dispersion and rapid electron fluctuations in the cusp: a case study, Ann. Geophys., 26, 2485–2502, 2008.

Markov, G.A., A.S. Belov, V.L. Frolov , V.O. Rapoport, M. Parrot, J.L. Rauch and M.T. Rietveld, Electromagnetic and plasma perturbations induced by radio emission of the EISCAT high-frequency heating facility in the outer ionosphere of the earth, Radiophysics and Quantum Electronics, 51, 11, doi:10.1007/s11141-009-9087-1, 2008.

Middleton, H. R., S. E. Pryse, A. G. Wood, and R. Balthazor, The role of the tongue-of-ionization in the formation of the poleward wall of the main trough in the European post-midnight sector, J. Geophys. Res., 113, A02306, doi:10.1029/2007JA012631, 2008.

Moen, J. I., Y. Rinne, H. C. Carlson, K. Oksavik, R. Fujii, and H. J. Opgenoorth, On the relationship between thin Birkeland current arcs and reversed flow channels in the winter cusp/cleft ionosphere, J. Geophys. Res., 113, A09220, doi:10.1029/2008JA013061, 2008.

Moen, J. X. C. Qiu, H. C. Carlson, R. Fujii, and I. W. McCrea, On the diurnal variability in F2-region plasma density above the EISCAT Svalbard radar, Ann. Geophys., 26, 2427–2433, 2008.

Næsheim, L. I., The PMSE Overshoot Effect, An Analysis of Campaign Data, Ph.D. Thesis, University of Tromsø, ISBN 978-82-92461-90-7, 2008.

Næsheim, L. I., O. Havnes, and C. La Hoz, A comparison of polar mesosphere summer echo at VHF (224

MHz) and UHF (930 MHz) and the effects of artificial electron heating, J. Geophys. Res., 113, D08205, doi:10.1029/2007JD009245, 2008.

Nesse, H., D. Heinrich, B. Williams, U.-P. Hoppe, J. Stadsnes, M. Rietveld, W. Singer, U. Blum, M. I. Sandanger, and E. Trondsen, A Case Study of a Sporadic Sodium Layer Observed by the ALOMAR Weber Na Lidar, Ann. Geophys., 26, 1071–1081, 2008.

Nygrén, T., M. Voiculescu, and A. T. Aikio, The role of electric field and neutral wind in the generation of polar cap sporadic E, Ann. Geophys., 26, 3757–3763, 2008.

Ogawa, Y., K. Seki, M. Hirahara, K. Asamura, T. Sakanoi, S. C. Buchert, Y. Ebihara, Y. Obuchi, A. Yamazaki, I. Sandahl, S. Nozawa, and R. Fujii, Coordinated EISCAT Svalbard radar and Reimei satellite observations of ion upflows and suprathermal ions, J. Geophys. Res., 113, A05306, doi:10.1029/2007JA012791, 2008.

Osepian, A., V. Tereschenko, P. Dalin, and S. Kirkwood, The role of atomic oxygen concentration in the ionization balance of the lower ionosphere during solar proton events, Ann. Geophys., 26, 131–143, 2008.

Oyama, S., B. J. Watkins, S. Maeda, H. Shinagawa, S. Nozawa, Y. Ogawa, A. Brekke, C. Lathuillere, and W. Kofman, Generation of the lower thermospheric vertical wind estimated with the EISCAT KST radar at high latitudes during periods of moderate geomagnetic disturbance, Annales Geophysicae 26(6), 1491—1505, 2008.

Pellinen-Wannberg, A., G. Wannberg, J. Kero, C. Szasz, and A. Westman, The impact of high resolution radar on meteor studies: the EISCAT perspective, Radio Science Bulletin, 324, 17–28, 2008.

Rapp, M., I. Strelnikova, R. Latteck, P. Hoffmann, U.-P. Hoppe, I. Häggström and M. T. Rietveld, Polar Mesosphere Summer Echoes (PMSE) studied at Bragg wavelengths of 2.8 m, 67 cm, and 16 cm, JASTP, 70,7 947–961, doi:10.1016/j.jastp.2007.11.005, 2008.

Renkwitz, Thomas, Analysis and Optimisation of Medium Gain X-Yagi Antennas for the EISCAT 3D 237.5MHz Incoherent Scatter Radar Active Array, Master's thesis, Universität Rostock, Fakultät für Informatik und Elektrotechnik, Institut für Nachrichtentechnik. 2008.

Rietveld, M. T., J. W. Wright, N. Zabotin, M. L. V. Pitteway, The Tromsø Dynasonde, Polar Science, 2, 1, 55–71, doi:10.1016/j.polar.2008.02.001, 2008.

Safargaleev, V., A. Kozlovsky, T. Sergienko, T. K. Yeoman, M. Uspensky, D. M. Wright, H. Nilsson, T. Turunen, and A. Kotikov, Optical, radar, and magnetic observations of magnetosheath plasma capture during a positive IMF Bz impulse, Ann. Geophys., 26, 517–531, 2008.

Senior, A., F. Honary, P. J. Chapman, M. T. Rietveld, T. S. Kelso, and M. J. Kosch, High-frequency magnetospheric sounding at EISCAT: some trials and their implications, Radio Sci., 43,RS4009, doi:10.1029/2007RS003779, 2008.

Senior, A., M. J. Kosch, and F. Honary, Comparison of methods to determine auroral ionospheric conductances using ground-based optical and riometer data, Ann. Geophys., 26, 3831–3840, 2008.

Sullivan, J. M., M. Lockwood, B. S. Lanchester, E. P. Kontar, N. Ivchenko, H. Dahlgren, and D. K. Whiter, An optical study of multiple NEIAL events driven by low energy electron precipitation, Ann. Geophys., 26, 2435–2447, 2008.

Szasz, Csilla, Radio meteors above the Arctic Circle: radiants, orbits and estimated magnitudes, PhD thesis, IRF Scientific Report 294, ISBN 978-91-977255-2-1, March 2008.

Szasz, C., J. Kero, D. D. Meisel, A. Pellinen-Wannberg, G. Wannberg and A. Westman, Orbit characteristics of the tristatic EISCAT UHF meteors, Monthly Notices of Royal Astronomical Society 388(1), 15–25, 2008.

Uspensky, M. V., R. J. Pellinen, and P. Janhunen, The electron drift velocity, ion acoustic speed and irregularity drifts in high-latitude E-region, Ann. Geophys., 26, 3395–3409, 2008.

Vierinen, J., M. S. Lehtinen, and I. I. Virtanen, Amplitude domain analysis of strong range and Doppler spread radar echos, Ann. Geophys., 26, 2419–2426, 2008.

Vierinen, J., M. S. Lehtinen, M. Orispää and I.I. Virtanen, Transmission code optimization method for incoherent scatter radar, Ann. Geophys., 26, 2923–2927, 2008.

Virtanen, I. I., M. S. Lehtinen, T. Nygrén, M. Orispää, and J. Vierinen, Lag profile inversion method for EISCAT data analysis, Ann. Geophys., 26, 571–581, 2008.

Virtanen, I. I., M. S. Lehtinen, and J. Vierinen, Towards multi-purpose IS radar experiments, Ann. Geophys., 26, 2281–2289, 2008.

Wannberg, Gudmund, EISCAT-3D: The Third Generation European Incoherent Scatter Radar System, Proceedings of Radio Science and Communications & Mathematical Modelling of Wave Phenomena (Eds. Sven Nordebo and Boerje Nilsson) , RVK08/MMWP08, ISSN 1650-2647, 140–144, 2008.

Wannberg, G., A. Westman, J. Kero, C. Szasz, and A. Pellinen-Wannberg, The EISCAT meteor code, Ann. Geophys., 26, 2303–2309, 2008.

Wood, A. G., Multi-instrument studies of polar cap patches in the high-latitude nightside ionosphere, PhD thesis, University of Wales, 2008.

Wood, A. G., S. E. Pryse, H. R. Middleton, and V. S. C. Howells, Multi-instrument observations of nightside plasma patches under conditions of IMF Bz positive, Ann. Geophys., 26, 2203–2216, 2008.

Wu, Z., B. Xu, J. Wu, and K. Xue, Incoherent scatter spectra of collisional plasma with the Lorentzian distribution, at URSI General Assembly, Chicago, 2008.

Xu, Bin, Jian Wu, Zhensen Wu, Jun Wu, Haiqin Che, Yubo Yan, and Kun Xue, Temperature enhancement induced by ionosphere heating in low altitude region, Progress in Natural Science 18(11), 1339—1343, 2008.

Xu, Bin, Kun Xue, Jian Wu, and ZhenSen Wu, Incoherent scatter spectra from plasma of a 13-moment approximation distribution function, Science in China Series E: Technological Sciences 51(5), 624—631, 2008.

Yin,P., C. N. Mitchell, P. Spencer, I. McCrea, and T. Pedersen, A multi-diagnostic approach to understanding high-latitude plasma transport during the Halloween 2003 storm, Ann. Geophys., 26, 2739–2747, 2008.

EISCAT Operations 2008

The EISCAT radars operate in two basic modes, using approximately half the available observing time for each. In the Special Programme mode, users conduct individual experiments dedicated to specific experiments and objectives. The resulting data are reserved for the exclusive use of the experimenters for one year from the date of collection. Special programmes often make use of the well developed pulse schemes and observing modes of the Common Programme. EISCAT Common Programmes are conducted for the benefit of the entire user community and the resulting data are immediately available to all. The common Programme modes are developed and maintained by EISCAT staff, and the overall programme is monitored by the Scientific Advisory Committee. Common Programme operations are often conducted as part of the coordinated World Day programme organised by the International Union of Radio Scientists (URSI) Incoherent Scatter Working Group (ISWG).

Common Programme One, CP-1, uses a fixed transmitting antenna, pointing along the geomagnetic field direction. The three-dimensional velocity and anisotropy in other parameters are measured by means of the receiving stations at Kiruna and Sodankylä (see map, inside front cover). CP-1 is capable of providing results with very good time resolution and is suitable for the study of substorm phenomena, particularly auroral processes where conditions might change rapidly. The basic time resolution is 5 s. Continuous electric field measurements are derived from the tri-static F-region data. On longer time scales, CP-1 measurements support studies of diurnal changes, such as atmospheric tides, as well as seasonal and solar-cycle variations. The observation scheme uses alternating codes for spectral measurements.

Common Programme Two, CP-2, is designed to make measurements from a small, rapid transmitter antenna scan. One aim is to identify wave-like phenomena with length and time scales comparable with, or larger than, the scan (a few tens of kilometers and about ten minutes). The present version consists of a four-position scan which is completed in six minutes. The first three positions form a triangle with vertical, south, and south-east positions, while the fourth is aligned with the geomagnetic field. The remote site antennas provide three-dimensional velocity measurements in the F-region. The pulse scheme is identical with that of CP-1.

Common Programme Three, CP-3, covers a 10° latitudinal range in the F-region with a 17-position scan up to 74°N in a 30 minute cycle. The observations are made in a plane defined by the magnetic meridian through Tromsø, with the remote site antennas making continuous measurements at 275 km altitude. The coding scheme uses alternating codes. The principle aim of CP-3 is the mapping of ionospheric and electrodynamic parameters over a broad latitude range.

Common Programmes One, Two, and Three are run on the UHF radar. Three further programmes are designed for use with the VHF system. The UHF and VHF radars are often operated simultaneously during the CP experiments. Such observations offer comprehensive data sets for atmospheric, ionospheric, and magnetospheric studies.

Common Programme Four, CP-4, covers geographic latitudes up to almost 80°N (77°N invariant latitude) using a low elevation, split-beam configuration. CP-4 is particularly suitable for studies of high latitude plasma convection and polar cap phenomena.

Common Programme Six, CP-6, is designed for low altitude studies, providing spectral measurements at mesospheric heights. Velocity and electron density are derived from the measurements and the spectra contain information on the aeronomy of the mesosphere. Vertical antenna pointing is normally used.

Common Programme Seven, CP-7, probes high altitudes and is particularly aimed at polar wind studies. The present version uses both of the VHF klystrons and is designed to cover altitudes up to 2500 km vertically above Ramfjordmoen.

Equivalent Common Programme modes are available for the EISCAT Svalbard Radar. CP-1 is directed along the geomagnetic field (81.6° in-

clination). CP-2 uses a four position scan. CP-3 is a 15 position elevation scan with southerly beam swinging positions. CP4 combines observations in the F-region viewing area with field-aligned and vertical measurements. Alternating code pulse schemes have been used extensively for each mode to cover ranges of approximately 80 to 1200 km with integral clutter removal below 150 km.

The tables on the next pages summarise the accounted hours on the various facilities for each month and for each Common Programme mode (CP) or Associate (SP).

KST COMMON PROGRAMMES

2008	Jan	Feb	Mar	Apr	May	Jun	Jul	Aug	Sept	Oct	Nov	Dec	Total	%	Target%
CP1		1	0.5	37		78.5	12	35.5	0.5	85			250	20	16
CP2	24	34	84	83	88	42		46	45	43.5	45	82	616.5	50	16
CP3							190		25.5	54	41.5		311	25	12
CP4											9.5		9.5	1	10
CP6								24					24	2	20
CP7	1	3											4	0	18
UP1	19.5												19.5	2	
UP2													0	0	
UP3													0	0	
Total	44.5	38	84.5	120	88	120.5	202	105.5	71	182.5	96	82	**1234.5**	100	
%	4	3	7	10	7	10	16	9	6	15	8	7	100		

KST SPECIAL PROGRAMMES

2008	Jan	Feb	Mar	Apr	May	Jun	Jul	Aug	Sept	Oct	Nov	Dec	Total	Incl AA	Target
CN	16					6	12.5						34.5	42	56
FI	9.5	44									76	37	166.5	180	95
GE						2	35				28.5		65.5	74	63
NI	13		41.5				3.5		11.5	17	41	10.5	138	155	120
NO	13.5	45	7		13	51.5	65			22	16.5		233.5	264	220
SW	42.5	21.5								24.5	22.5	12	123	145	160
UK	34	42.5	171	14		14	24.5						300	323	164
AA	20	30	16	16	6			13.5	21.5				123		
Total	148.5	183	235.5	30	19	73.5	140.5	13.5	33	63.5	184.5	59.5	**1184**	**1184**	**878**
%	13	15	20	3	2	6	12	1	3	5	16	5	100		

	EI	CN	FI	GE	NI	NO	SW	UK	
Target		6.38	10.85	7.15	13.63	25.01	18.25	18.73	%

KST OTHER PROGRAMMES

2008	Jan	Feb	Mar	Apr	May	Jun	Jul	Aug	Sept	Oct	Nov	Dec	Total	Target
3P				13.5		12				9			34.5	71
EI									0.5	0.5		1	2	31
TNA			36			12	16					63	127	120
IPY													0	
TB											54	18.5	72.5	73
Total	0	0	36	13.5	0	24	16	0	0.5	9.5	54	82.5	**236**	**295**

KST CUMULATIVE TOTALS

2008	Jan	Feb	Mar	Apr	May	Jun	Jul	Aug	Sept	Oct	Nov	Dec	Total	Target
CP	44.5	38	84.5	120	88	120.5	202	105.5	71	182.5	96	82	1234.5	469
SP	148.5	183	235.5	30	19	73.5	140.5	13.5	33	63.5	184.5	59.5	1184	878
OP	0	0	36	13.5	0	24	16	0	0.5	9.5	54	82.5	236	295
Total	193	221	356	163.5	107	218	358.5	119	104.5	255.5	334.5	224	**2654.5**	**1642**

USAGE BREAKDOWN

2008	Jan	Feb	Mar	Apr	May	Jun	Jul	Aug	Sept	Oct	Nov	Dec	Total	Target
UHF	68	95.5	174.5	80.5	58.5	109.5	186	51.5	53.5	154	156	118	1305.5	666
VHF	95	55	16	17	6	32		43.5	21.5	8	101.5		395.5	316
Heating	9	31.5	16	13.5	18	31.5	40.5		4.5	27.5	17.5	4	213.5	168
Passive UHF	82.5	168.5	333.5	223	117.5	178	282.5	96	119	267.5	240	194	2302	1968
ESR	684.5	651.5	124.5	116	85	137.5	94	23	0	209.5	220	197	2542.5	2669
Passive ESR			10	38									48	

ESR COMMON PROGRAMMES

2008	Jan	Feb	Mar	Apr	May	Jun	Jul	Aug	Sept	Oct	Nov	Dec	Total	%	Target%
CP1				44.5	0.5	50	16	11		83			205	39	54
CP2					60.5	30				30	30	55.5	206	39	16
CP3					2		55.5				54		111.5	21	12
CP4													0	0	10
CP6								6					6	1	
CP7													0	0	
UP1													0	0	
UP2													0	0	
UP3													0	0	
Total	0	0	0	44.5	63	80	71.5	17	0	113	84	55.5	**528.5**	100	
%	0	0	0	8	12	15	14	3	0	21	16	11	100		

ESR SPECIAL PROGRAMMES

2008	Jan	Feb	Mar	Apr	May	Jun	Jul	Aug	Sept	Oct	Nov	Dec	Total	Incl AA	Target
CN													0	5	54
FI	24.5										21	11	56.5	65	91
GE					6.5	44							50.5	56	60
NI	7						22.5			2.5	32.5	23	87.5	99	115
NO	9	25								58.5	5.5	10.5	108.5	129	211
SW	35											46.5	81.5	96	154
UK	37.5	12	51	9.5						23			133	148	158
AA	15	30	16.5	12	7.5								81		
Total	128	67	67.5	21.5	14	44	22.5	0	0	84	59	91	**598.5**	**599**	**843**
%	21	11	11	4	2	7	4	0	0	14	10	15	100		

ESR OTHER PROGRAMMES

2008	Jan	Feb	Mar	Apr	May	Jun	Jul	Aug	Sept	Oct	Nov	Dec	Total	Target
3P	1.5	23			8	8				12.5			53	57
EI													0	25
TNA	5												5	
IPY	550	561.5	59.5	59.5									1230.5	1230
TB						5.5		6			77	50.5	139	139
Total	556.5	584.5	59.5	59.5	8	13.5	0	6	0	12.5	77	50.5	**1427.5**	**1451**

ESR CUMULATIVE TOTALS

2008	Jan	Feb	Mar	Apr	May	Jun	Jul	Aug	Sept	Oct	Nov	Dec	Total	Target
CP	0	0	0	44.5	63	80	71.5	17	0	113	84	55.5	528.5	375
SP	128	67	67.5	21.5	14	44	22.5	0	0	84	59	91	598.5	843
OP	556.5	584.5	59.5	59.5	8	13.5	0	6	0	12.5	77	50.5	1427.5	1451
Total	684.5	651.5	127	125.5	85	137.5	94	23	0	209.5	220	197	**2554.5**	**2669**

List of meetings, 2008

EISCAT Annual Review Meeting

ARM 2008 12–14 March, 2008, Skibotnsenteret, Norway

EISCAT Council

Council 70th 27–28 May 2008, Swedish Institute of Space Physics, Kiruna, Sweden

Council 70th-extra 4–5 September 2008, Best Western Hotel City, Copenhagen, Denmark

Council 71st 30–31 October 2008, Kun Ming Wah Plaza International Hotel, P. R. of China

EISCAT Management Committee

EMC 03 15 February 2008, Teleconference

EISCAT Scientific Oversight Committee

SOC 02 22–24 April 2008, Polar Research Institute of China, Shanghai, P. R. of China

SOC 03 2–3 September 2008, Ångströmlaboratoriet, Uppsala, Sweden

EISCAT_3D Project Meetings

GA5 16 January 2008, Fifth General Assembly Meeting, Arlanda, Stockholm, Sweden

SG6 12 February 2008, Sixth Steering Group Meeting, Arlanda, Stockholm, Sweden

GA6 11 March 2008, Sixth General Assembly Meeting, Teleconference

SG7 4 April 2008, Seventh Steering Group Meeting, Teleconference

GA7 10 April 2008, Seventh General Assembly Meeting, Teleconference

AH3 16-17 September 2008, Third All-Hands Meeting, Swedish Institute of Space Physics, Kiruna, Sweden

SG8 17 September 2008, Eighth Steering Group Meeting, Swedish Institute of Space Physics, Kiruna, Sweden

GA8 22 December 2008, Eighth General Assembly Meeting, Mailconference

Staff celebrations, 2008

ARM 2008

2 years (Silver Pin) Stian Grande, Tromsø

10 years (Plate) Kjellfrid Ingebrigtsen, Tromsø

Other

Glass Sculpture Tony van Eyken leaving EISCAT
31 December 2008

Beynon medals

The EISCAT Council awards distinguished persons the Sir Granville Beynon medal.

Recipients

1st Prof. Tor Hagfors 2002 Awarded to Professor Tor Hagfors on 4th February 2002 for his outstanding services to the EISCAT Scientific Association and to Ionospheric Physics

2nd Prof. Tauno Turunen 2003 In recognition of important contributions to the techniques of Incoherent Scatter Radar and outstanding services to the EISCAT Scientific Association

3rd Prof. Jürgen Röttger 2004 In recognition of outstanding services to the EISCAT Scientific Association including the establishment of the EISCAT Svalbard Radar at Longyearbyen

4th Prof. Henry Rishbeth 2006 Awarded by the Council of the EISCAT Scientific Association to Professor Henry Risbeth. In recognition of outstanding contributions to the scientific exploitation of incoherent scatter in Europe including the UK PUSCAT and MISCAT radars and the radars of the EISCAT Scientific Association

5th Prof. Nobuo Matuura 2007 Awarded by the Council of the EISCAT Scientific Association to Professor Nobuo Matuura. In recognition of his contributions to the successful establishment of the EISCAT Svalbard Radar at Longyearbyen and to the expansion of the EISCAT Scientific Association to include non-European members

6th Prof. Markku Lehtinen 2008 Awarded by the Council of the EISCAT Scientific Association to Professor Markku Lehtinen. In recognition of his seminal contributions to the development of advanced modulation techniques for incoherent scatter radars and to the mathematical foundations and implementation of effective incoherent scatter radar data analysis systems

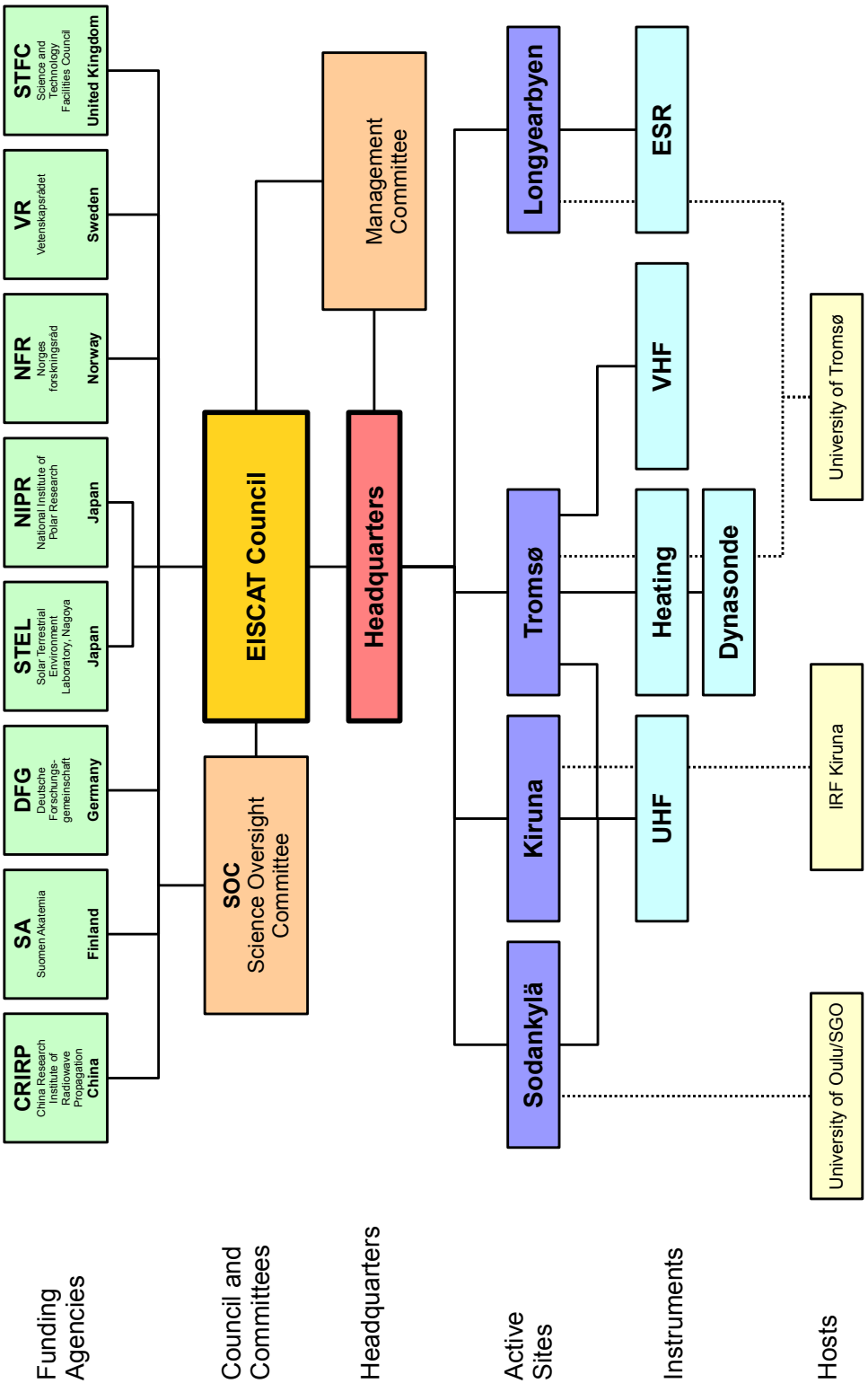

EISCAT organisational diagram, December 2008.

EISCAT Scientific Association

December 2008

Council

The Council consists of a Delegation of each Associate with a maximum of three persons from each Associate.

Finland	
Dr. S. Hemming	Delegate
Dr. K. Kauristie	*Vice-Chairperson*
Prof. T. Nygrén	
Germany	
Dr. H. Boos	Delegate
Prof. J. Röttger	
Japan	
Prof. R. Fuiji	Delegate
Dr. H. Miyaoka	
Norway	
Prof. A. Brekke	*Chairperson*
Dr. B. Jacobsen	Delegate
Mr. L. Lønnum	
Sweden	
Dr. T. Andersson	Delegate
Dr. A. Pellinen-Wannberg	
P. R. of China	
Prof. Q. Dong	Delegate
Prof. J. Wu	
United Kingdom	
Dr. I. McCrea	
Ms. R. Young	Delegate
Staff Representative	
Mr. P. Bergqvist	

Scientific Oversight Committee

Under the guidance of the Council, the EISCAT scientific community will organise a Scientific Oversight Committee.

Dr. A. Aikio	Finland
Dr. S. Buchert	Sweden
Dr. J. Chao	External member
Dr. S. Gonzales	External member
Dr. M. Kosch	*Chairperson*, United Kingdom
Prof. C. La Hoz	Norway
Prof. R. Liu	*Vice-Chairperson*, P. R. of China
Prof. S. Nozawa	Japan
Prof. J. Röttger	Germany

Director

Prof. A. P. van Eyken

Management Committee

The Management Committee shall normally be composed of the Director and four members appointed by the Council.

Dr. D. Alcaydé	External Member
Dr. T. Andersson	Council Member
Prof. A. P. van Eyken	*Chairperson*, Director
Dr. K. Kauristie	Council Vice-Chairperson

Executives

Senior Management

Mr. H. Andersson	Head of Adm., Deputy Dir.
Prof. A. P. van Eyken	Director

Site Leaders

Station Managers

Mr. H. Boholm	EISCAT Svalbard Radar
Mr. R. Jacobsen	Tromsø Radar
Mr. M. J. Postila	Sodankylä Site
Dr. M. T. Rietveld	Tromsø Heating
Mr. L.-G. Vanhainen	Kiruna Site

EISCAT staff at the Annual Review Meeting, 12–14 March 2008, at Skibotnsenteret, Norway.

Appendix:

EISCAT Scientific Association Annual Report, 2008

EISCAT Scientific Association
Registered as a Swedish non-profit organisation
Organisation number: 897300-2549

Annual report for the financial year 2008-01-01 – 2008-12-31

The EISCAT Council and the Director for the Association herewith submits the annual report for 2008.

ADMINISTRATION REPORT

Ownership, organisation and objective
The EISCAT Scientific Association was established in 1975 through an agreement between six European organisations. Japan joined in 1996 and the Peoples Republic of China in 2007.

The current EISCAT Associates are: China Research Institute of Radiowave Propagation (Peoples Republic of China), Deutsche Forschungsgemeinschaft (Germany), National Institute of Polar Research (Japan), Norges forskningsråd (Norway), Science and Technology Facilities Council (United Kingdom of Great Britain and Northern Ireland), Solar-Terrestrial Environment Laboratory, Nagoya University (Japan), Suomen Akatemia (Finland), and Vetenskapsrådet (Sweden).

A new EISCAT Agreement came into force 2007-01-01, with all Associates making long term funding commitments to the Association. The Association has its formal seat in Kiruna, Sweden, and is registered as a non-profit organisation.

The aim of the Association is to make significant progress in the understanding of physical processes in the high latitude atmosphere by means of experimental programmes generally conducted using the incoherent scatter radar technique, which may be carried out as part of wider international projects. For this purpose, the Association has developed, constructed, and now operates, a number of radar facilities at high latitudes. At present, these comprise a system of stations at Tromsø (Norway), Kiruna (Sweden), Sodankylä (Finland), and Longyearbyen (Svalbard).

The Association is fully funded by the Associates but additional operations may also be funded by short term additional contributions from both Associate and non-Associate bodies. Depending on the available funding, scientific priorities and operational targets are adjusted on an annual basis.

The EISCAT Council is charged with the overall administration and supervision of the Association's activities. The Council appoints a Director, who is responsible for the daily management and operation of the facilities of the Association.

The Council have appointed a new Director, Dr. Esa Turunen, who started 2009-01-01. The previous Director, Professor Anthony P. van Eyken continued in office until his employment ended 2008-12-31.

Operation and scientific development
The EISCAT Radars delivered a full programme of operations for the user community and operated reliably throughout the year with only minor interruptions due to equipment or operational problems.

The various EISCAT radars operated for a total of 5 209 accounted hours (7 708 hours in 2007), compared with a revised target of 4 535 hours. Included in these totals is the final

part of the year-long IPY run that commenced 2007-03-01 and ended 2008-02-29. After the first year, the IPY run continued in a bi-weekly type of routine observations to cover the second IPY year. On average, about 100 hours of IPY measurements have been performed per month starting from March 2008.

Common Programmes amounted to 34% (7%) of the operations. Special Programmes amounted to 34% (24%) and the IPY run plus other operations amounted to 32% (69%) of the total run hours.

A contract, under the European Union's Sixth Framework Programme initiative - Structuring the European Research Area – Design Studies, continued throughout the year. The project, EISCAT_3D underwent a major project revision during the year where the consortium was expanded and tasks and efforts were redistributed. The project started 2005-05-01 and will end 2009-04-30. About 2.3 staff-years were invested in the project during the year.

A major achievement was reached when the EISCAT_3D concept was included in the European Strategy Forum on Research Infrastructures (ESFRI) updated 2008 Research Infrastructure Roadmap.

The second European Union, Sixth Framework Programme initiative, project continued providing Transnational Access to the facilities. Four user groups visited the Tromsø facility and performed their own experiments during the year. Totally 92 hours were accounted, and paid by EU. The visitors travel expenses were also paid by EU funds.

The VHF radar continued to operate with a single klystron. The sealant issue is still of concern. Industry professionals have suggested ways to overcome the problem but the implementation has been postponed mainly due to the operations schedule.

French scientists have continued to use the facilities, running 206 hours during the year, and have been invoiced for the hours used.

An agreement with the Arctic and Antarctic Research Institute (AARI), Russian Federation, was signed in October allowing AARI scientists to use the facilities against an hourly rate. AARI did the first payment in November covering operations 2008-12-01 – 2009-11-30.

Ukraine stated in 2005 that they would join the Association in 2008. The joining process was delayed but is now envisaged to be completed in 2009. The scientific collaboration has meanwhile continued and Ukrainian scientists have made use of the facilities.

The annual staff review meeting was held in Skibotn, Norway, mid March. EISCAT scientists attended several international conferences during the year, including CEDAR (USA), COSPAR (Canada), EGU (Austria) URSI (USA), ISSI workshops (Switzerland), RVK (Sweden), Icestar (Norway), as well as national gatherings.

Future operation and scientific development

During the coming year, EISCAT will continue to support the wide range of existing and new programmes proposed by the various Associates' scientific communities, including the hosting of user-supplied equipment.

Some operations emphasis will be put on the UHF tristatic system due to the uncertain future of UHF frequency availability after 2009. The Svalbard system has now returned to a more normal operation pattern after the substantial IPY runs.

The EISCAT_3D design study will end in April 2009 and work has started to seek funds for the next project, the preparatory phase ESFRI concept system. The Transnational Access project is into its last year and in order to come closer to the project target, the project management has been refocused and an extra late-spring application round been added.

The work of the Council and its committees

The Council had two ordinary and one extraordinary meeting under the leadership of the Chairperson, Professor Asgeir Brekke: in May, Kiruna, Sweden, in September, the extraordinary meeting, Copenhagen, Denmark, and in October, Council met in Kunming, P. R. of China. The management committee had one teleconference meeting in February. The Scientific Oversight Committee had two meetings during the year: April, Shanghai, P. R. of China and October, Uppsala, Sweden.

Council decided already in 2007 to change the management structure, including not renewing the Director contract, which would run out at the end of 2008. To implement this, settlement agreements were agreed during the year with the Deputy Director and the Director. The Deputy Director left 2008-02-29 and the Director left 2008-12-31.

The Director search committee, a Council established group, continued its work and presented the findings at the extraordinary Council meeting. After consideration, Council decided to offer the Director position to Dr. Esa Turunen, then working at the Sodankylä Geophysical Observatory.

Council and Dr. Turunen signed the employment contract at the Kunming meeting. The employment is for three years, 2009-01-01 – 2011-12-31. Dr. Turunen has his office at Headquarters, Kiruna, Sweden and he is under Swedish employment and taxation rules. His salary is in SEK.

At the Kunming meeting, Council endorsed the EISCAT_3D concept by resolving that the development of new radar facilities capable of three-dimensional volumetric imaging of the atmosphere and ionosphere is an essential requirement for the future of the association, since this satisfies user demands for deeper insights into applications such as middle atmosphere science, multi-scale coupling, electrodynamics, meteors and space debris studies.

Council did also support the proposal to have a staff representative participating in Council meetings and staff was represented both at the extraordinary and the Kunming meeting.

At the end of the year, the Council Chairpersonship was taken over by Dr. Kirstie Kauristie, Finland. She will serve for initially two years.

Budget development during the year

The 2008 operations ended a bit over the revised target. This was a deliberate overrun and it has produced excellent output data. Some further investments were made than budgeted. Both actions were possible because of improved funding. Altogether, the regular budget development was acceptable and in accordance with plans. The weakened SEK currency was capitalised in December by converting primarily received EUR contributions to SEK. Bank interests produced good income for most of the year. French and Russian payments improved the contributions situation. These improvements could not fully compensate for the Council made Director settlement agreements and resulting costs. The year ended in a deficit which had to be covered by own reserves.

The long-term budget plan

The long-term budget plan remains feasible. The five years plan is balanced up to 2012. The annual operating hours level will be around 2 600 hours. The annual staff complement will amount to about 20 persons.

The result for 2008 and the deficit handling

The year was balanced by covering the deficit, 1 295 kSEK, from the Restructuring reserve.

PROFIT AND LOSS ACCOUNTS

in thousands of Swedish Crowns

	Note 1	***2008***	***2007***
Associate contributions	Note 2	23 611	23 944
Other operating income		8 592	4 718
		32 203	28 662
Operation costs		-6 361	-6 040
Administration costs		-4 253	-4 510
Personnel costs	Note 3	-23 956	-18 582
Depreciation of fixed assets		-5 026	-6 843
		-39 596	-35 975
Operating profit/loss		*-7 393*	*-7 313*
Interest income		866	788
Other financial income and cost		351	119
Own reserves and funds	Note 4	-145	1 646
		1 072	2 553
Profit/loss after financial items		*-6 321*	*-4 760*
Appropriations	Note 5	1 295	-2 083
Transfer from funds invested	Note 6	5 026	6 843
		6 321	4 760
Net profit/loss for the year		*0*	*0*

BALANCE SHEET

in thousands of Swedish Crowns

		2008	*2007*
ASSETS			
Fixed assets			
Tangible fixed assets	Note 7		
Buildings		3 995	4 281
Radar systems		2 041	5 992
Equipment and tools		1 643	1 636
		7 679	11 909
Current assets			
Receivables		1 723	2 601
Prepayments and accrued income	Note 8	610	616
Cash at bank and in hand	Note 9	20 370	32 909
		22 703	36 126
Total assets		*30 383*	*48 035*
CAPITAL AND LIABILITIES			
Capital			
Funds invested	Note 10	7 108	11 304
Funds held on reserve	Note 11	16 053	18 146
		23 161	29 449
Long term liabilities			
Long term liabilities	Note 12	509	577
Current liabilities			
Liabilities, trade	Note 13	4 768	17 267
Provisions	Note 14	37	0
Other liabilities		1 908	742
		6 713	18 009
Total capital and liabilities		*30 383*	*48 035*
Pledged assets		*509*	*577*
Contingent liabilities		*none*	*none*

STATEMENT OF CASH FLOWS

in thousands of Swedish Crowns

	2008	***2007***
Operating activities		
Operating result before financial items	-7 393	-7 313
Transfer from funds invested	5 026	6 843
Interest received	866	788
Currency exchange rate changes	314	13
Extra ordinary income and cost	37	106
Increase/decrease of receivables	878	-1 418
Increase/decrease of prepayments and accrued income	5	-34
Increase/decrease of creditors and liabilities	-11 364	6 081
Cash flow from operations	*-11 631*	*5 065*
Investment activities		
Investments in tangible assets	-908	-551
Cash flow from investment activities	*-908*	*-551*
Cash flow for the year	*-12 539*	*4 514*
Liquid assets at the beginning of the year	*32 909*	*28 395*
Liquid assets at the end of the year	*20 370*	*32 909*

NOTES

Note 1 *Accounting principles*

The accounting and valuation principles applied are consistent with the provisions of the Swedish Annual Accounts Act and generally accepted accounting principles (bokföringsnämnden allmänna råd och vägledningar).

All amounts are in thousands of Swedish kronor (SEK) unless otherwise stated.

Receivables
Receivables are stated at the amounts estimated to be received, based on individual assessment.

Receivables and payables in foreign currencies
Receivables and payables in foreign currencies are valued at the closing day rate. Where hedging measures have been used, such as forwarding contracts, the agreed exchange rate is applied. Gains and losses relating to operations are accounted for under other financial income and cost.

Bank accounts in foreign currencies
Bank balances in foreign currencies are valued at the closing day rate.

Fixed assets
Tangible fixed assets are stated at their original acquisition values after deduction of depreciation according to plan. Assets are depreciated systematically over their estimated useful lives. The following periods of depreciation are applied: Buildings 10 - 50 years, Radar systems 3 - 20 years and Equipment and tools 3 - 5 years.

Note 2 *Associate contributions*

The Associates contributed to the operation during the year in accordance with the agreement. The commitments are in local currencies. The received contributions have been accounted in SEK.

	2008
CRIRP (P. R. of China)	2 422
DFG (Germany)	1 697
NIPR (Japan)	1 294
RCN (Norway)	5 574
SA (Finland)	3 307
STFC (United Kingdom)	3 918
VR (Sweden)	5 400
	23 611

Accumulated contributions status as of 2008-12-31

	1976 - 2008
Previous Associates	190 074
CRIRP (P. R. of China)	7 480
DFG (Germany)	186 785
NIPR (Japan)	65 083
RCN (Norway)	128 366
SA (Finland)	54 821
STFC (United Kingdom)	210 352
VR (Sweden)	102 402
	945 362

Note 3 *Personnel costs and average number of employees*

The Association employs directly the Headquarters staff, currently about six positions, including the Director. The Headquarters is located in Kiruna, Sweden. The personnel working at the Kiruna (Sweden), Sodankylä (Finland), Svalbard and Tromsö (Norway) sites are not employed by the Association. Instead, the personnel are provided via site contracts by the Swedish Institute of Space Physics (Kiruna site staff), Oulu University (Sodankylä staff) and Tromsö University (Tromsö and Svalbard staff). The Association refunds all expenses related to the provided staff, as well as an additional overhead.

	2008	***2007***
Personnel costs in total		
Salaries and emoluments paid to the Directors	6 583	2 240
Other personnel, employed and provided via site contracts	11 472	11 627
Social security contributions amounted to	4 717	3 996
of which for pension costs	3 170	2 442

The Council concluded settlement arrangements with both Director's resulting in that the Deputy Director left 2008-02-29 and the previous Director left 2008-12-31. The settlements included one-off severance pay, 4 778 kSEK, one-off pension payment, 885 kSEK and ongoing funding committments until 2011-02-28. The ongoing committment, not included in Director salaries above, costed 459 kSEK.

Of the pension costs, 1 660 kSEK (1 021 kSEK) relates to the Directors. The Directors and all other directly employed staff are included in ITP like occupational pension plans. For the personnel provided via site contracts, the pension plans are handled by their respective employer.

The members of the board (EISCAT Council) and members of committees, who represents Associates, do not receive remunerations from the Association. Travel expenses in connection with Council and committee meetings are normally covered by the Associates.

Salaries and emoluments and average number of staff per country

Finland		
Salaries and emoluments	1 767	1 560
Average number of staff - men and women	4 + 0	4 + 0
Norway (including Svalbard)		
Salaries and emoluments	12 033	8 111
Average number of staff - men and women	10 + 1	10 + 0
Sweden		
Salaries and emoluments	4 255	4 195
Average number of staff - men and women	6 + 1	6 + 2

Members of the board and Directors at year-end - men and women

Board members (EISCAT Council)	12 + 4	12 + 4
Directors	2 + 0	2 + 0

Note 4 *Own reserves and funds*

Transactions involving own reserves and funds.

Capital Operating reserve		
Budgeted transfer to the reserve	-396	-353
Transfer from the reserve	908	551
Investments made	-942	-580
External projects reserve		
Design study: balancing the four-year project	-675	-435
Restructuring reserve		
Budgeted restructuring costs	1 355	1 380
Spare parts reserve		
Budgeted transfer to the reserve	-27	-30
Transfer from the reserve	9	32

	2008	2007
Surplus fund		
Budgeted transfer from the fund	3 685	2 683
Budgeted transfer to the fund	-4 062	-1 602
Sum own reserves and funds	*-145*	*1 646*

Note 5 *Appropriations*

The outcome for this year became a deficit relative to the budget amounting to 1 295 kSEK. The deficit was covered by funds from the Restructuring reserve. The 2007 outcome resulted in a surplus (2 083 kSEK) and it was transferred to the Surplus fund.

Note 6 *Transfer from funds invested*

The depreciation cost is covered by funds from Capital - funds invested

Note 7 *Tangible fixed assets*

Changes in tangible fixed assets during 2008.

Buildings		
Opening acquisition value	42 237	42 204
Acquisitions during the year	0	33
Disposals during the year	0	0
Closing acquisition value	42 237	42 237
Opening accumulated depreciation	-37 956	-37 448
Depreciations during the year	-286	-508
Disposals during the year	0	0
Closing accumulated depreciation	-38 242	-37 956
Closing residual value	3 995	4 281
Radar systems		
Opening acquisition value	244 381	244 381
Acquisitions during the year	0	0
Disposals during the year	0	0
Closing acquisition value	244 381	244 381
Opening accumulated depreciation	-238 389	-232 901
Depreciations during the year	-3 951	-5 488
Disposals during the year	0	0
Closing accumulated depreciation	-242 340	-238 389
Closing residual value	2 041	5 992
Equipment and tools		
Opening acquisition value	31 078	31 902
Acquisitions during the year	908	518
Disposals during the year	-61	-1 342
Closing acquisition value	31 925	31 078
Opening accumulated depreciation	-29 442	-29 936
Depreciations during the year	-789	-847
Disposals during the year	-52	1 341
Closing accumulated depreciation	-30 283	-29 442
Closing residual value	1 643	1 636
Sum tangible fixed assets	*7 679*	*11 909*

	2008	2007

Note 8 *Prepayments and accrued income*

The main buildings and systems insurance for 2008 was paid in December.

Prepaid rents	92	89
Prepaid insurances	492	511
Other items	26	16
	610	616

Note 9 *Bank balances status*

Nordea	20 369	32 907
Cash in hand	1	2
	20 370	32 909

Note 10 *Funds invested status*

Buildings	3 424	3 676
Radar Systems	2 041	5 992
Equipment and Tools	1 643	1 636
	7 108	11 304

Note 11 *Funds held on reserve*

Investments were made to a larger extent than budgeted. The overuse, 512 kSEK, was covered by the Capital operating reserve. 675 kSEK was transferred to the External project reserve for later use in the four-year EU supported EISCAT_3D design study project (ending 2009-04-30). The outcome deficit, 1 295 kSEK, was covered by funds from the Restructuring reserve.

Capital operating reserve	1 223	1 735
Equipment repair fund	754	754
External projects reserve	1 504	829
Investment fund	2 556	2 556
Restructuring reserve	5 601	8 252
Spare parts reserve	353	335
Surplus fund	4 062	3 685
	16 053	18 146

Note 12 *Long term liabilities*

Refers to the Husbanken Norway loan concerning the owned flat on Svalbard. The loan is in NOK. 34 kSEK (29 kSEK) was amortized during the year.

Note 13 *Liabilities, trade*

Two EU-contracts are running, the EISCAT_3D Design Study and the EISCAT_USERS_1 Transnational access project. The design study started 2005-05-01. The other project started 2006-01-01. Both projects work with pre-financing. The EISCAT_3D prefinancing funds were distributed to the project consortium during the year. Non released funds are accounted as liabilities.

Liabilities EU, EISCAT_3D pre-financing	0	9 747
Liabilities EU, USERS_1 pre-financing	913	1 470
Other liabilities, trade	3 855	6 050
	4 768	17 267

Note 14 *Provisions*

The EISCAT Council had an extra-ordinary meeting in Copenhagen. The meeting were held in a non-Associate country and the venue cost will therefore be paid by the Association.

Council cost	37	0

Berlin 2009-06-03

Dr. Tomas Andersson

Dr. Heike Boos

Prof. Ryoichi Fujii

Dr. Bjørn Jacobsen

Dr. Tuukka Lehtiniemi

Ms. Rosemary Young

Prof. Jian Wu

Dr. Esa Turunen
Director

Our audit report was issued on 2009-06-24

Mrs. Annika Wedin
Authorised Public Accountant

Öhrlings
PRICEWATERHOUSECOOPERS

Audit report

To the council of EISCAT Scientific Association

Corporate identity number 897300-2549

I have audited the annual accounts, the accounting records and the administration of the council and the director of EISCAT Scientific Association for the year 2008. These accounts and the administration of the association and the application of the Annual Accounts Act when preparing the annual accounts are the responsibility of the council and the director. My responsibility is to express an opinion on the annual accounts and the administration based on my audit.

I conducted my audit in accordance with generally accepted auditing standards in Sweden. Those standards require that I plan and perform the audit to obtain reasonable assurance that the annual accounts are free of material misstatement. An audit includes examining, on a test basis, evidence supporting the amounts and disclosures in the accounts. An audit also includes assessing the accounting principles used and their application by the council and the director and significant estimates made by the council and the director when preparing the annual accounts as well as evaluating the overall presentation of information in the annual accounts. As a basis for my opinion concerning discharge from liability, I examined significant decisions, actions taken and circumstances of the association in order to be able to determine the liability, if any, to the council or the director. I also examined whether any council member or the director has, in any other way, acted in contravention of the Annual Accounts Act or the statutes. I believe that my audit provides a reasonable basis for my opinion set out below.

The annual accounts have been prepared in accordance with the Annual Accounts Act and give a true and fair view of the association's financial position and results of operations in accordance with generally accepted accounting principles in Sweden.
The statutory administration report is consistent with the other parts of the annual accounts.

The council and the director have not acted in contravention of the statutes.

Gävle, 29 June 2009

Annika Wedin
Authorized Public Accountant

Report 2008 of the EISCAT Scientific Association

EISCAT Headquarters
Box 812, SE-981 23 Kiruna, Sweden

Scientific contributions: EISCAT Associates and staff

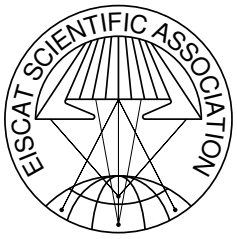

The EISCAT Associates

December 2008

CRIRP

China Research Institute of Radiowave Propagation
China
www.crirp.ac.cn

SA

Suomen Akatemia
Finland
www.aka.fi

DFG

Deutsche Forschungsgemeinschaft
Germany
www.dfg.de

STEL

Solar Terrestrial Environment Laboratory, Nagoya
Japan
www.stelab.nagoya-u.ac.jp

NIPR

National Institute of Polar Research
Japan
www.nipr.ac.jp

NFR

Norges forskningsråd
Norway
www.forskningsradet.no

VR

Vetenskapsrådet
Sweden
www.vr.se

STFC

Science and Technology Facilities Council
United Kingdom
www.scitech.ac.uk

EISCAT Scientific Association

Headquarters

EISCAT Scientific Association
Box 812
SE-981 28 Kiruna, Sweden
Phone: +46-980-79150
Fax: +46-980-79159
Email: eiscat@eiscat.se
www.eiscat.se

Sites

Kiruna

EISCAT
Swedish Institute of Space Physics
Box 812
SE-981 28 Kiruna, Sweden
Phone: +46-980-79136
Fax: +46-980-29276
Email: eiscat@eiscat.irf.se

Sodankylä

EISCAT
Tähteläntie 54B
FIN-99600 Sodankylä, Finland
Phone: +358-16-619880
Fax: +358-16-610375
Email: eiscat@eiscat.sgo.fi

Tromsø

EISCAT
Ramfjordmoen
N-9027 Ramfjordbotn, Norway
Phone: +47-776-20730
Fax: +47-776-20740
Email: eiscat@eiscat.uit.no

Longyearbyen

EISCAT Svalbard Radar
Postboks 432
N-9171 Longyearbyen, Svalbard
Phone: +47-790-21236
Fax: +47-790-21751
Email: eiscat@esr.eiscat.no